Indoor MIMO Channels with Polarization Diversity: Measurements and Performance Analysis

A Thesis
Presented to
The Academic Faculty

by

Vikram R. Anreddy

In Partial Fulfillment
of the Requirements for the Degree
Master of Science in Electrical and Computer Engineering

School of Electrical and Computer Engineering
Georgia Institute of Technology
May 2006

Indoor MIMO Channels with Polarization Diversity: Measurements and Performance Analysis

Approved by:

Professor Mary Ann Ingram, Adviser
School of Electrical and Computer Engineering
Georgia Institute of Technology

Professor Douglas B. Williams
School of Electrical and Computer Engineering
Georgia Institute of Technology

Professor Gregory David Durgin
School of Electrical and Computer Engineering
Georgia Institute of Technology

Date Approved: April 10, 2006

To my parents

Shobha and Ranga Anreddy

ACKNOWLEDGEMENTS

First and foremost, I wish to express my deepest sense of gratitude to my adviser, Prof. Mary Ann Ingram. She has provided me with invaluable support and guidance during my graduate studies. I am grateful to her for the faith she has shown in my abilities and for her patience and understanding, without which this thesis would not have been possible.

I also thank Prof. Gregory Durgin and Prof. Douglas Williams, for serving on my thesis committee and for their critical review of this work.

I have enjoyed working with my colleagues, past and present, in the Smart Antennas Research Laboratory. I would like to thank them all for their help, encouragement and for the many fruitful discussions we have had over the past two years.

Outside the sphere of my lab, I have been fortunate to befriend some very interesting people at Georgia Tech. I thank them all for their friendship. A special thanks to my cousins in Atlanta, for all their affection and support.

Above all, I thank my parents for their love and affection. Thanks to my brother, who has been a very good friend and a real source of inspiration. But for the encouragement and support of my family, I would never have got so far in my career.

TABLE OF CONTENTS

LIST OF TABLES

LIST OF FIGURES

SUMMARY

This thesis deals with dual-polarized multiple input multiple output (MIMO) channels, an important issue for the practical deployment of multiple antenna systems. The MIMO architecture has the potential to dramatically improve the performance of wireless systems. Much of the focus of research has been on uni-polarized spatial MIMO configurations, the performance of which, is a strong function of the inter-element spacing. Thus the current trend of miniaturization, seems to be at odds with the implementation of spatial configurations in portable handheld devices. In this regard, dual-polarized antennas present an attractive alternative for realizing higher order MIMO architectures in compact devices.

Unlike spatial channels, in the presence of polarization diversity, the subchannels of the MIMO channel matrix are not identically distributed. They differ in terms of average received power, envelope distributions, and correlation properties. In this thesis, we report on an indoor channel measurement campaign conducted at 2.4 GHz, to measure the co-polarized and cross-polarized subchannels, under line-of-sight (LOS) and non-line-of-sight (NLOS) channel conditions. The measured data is then analyzed, to draw a fair comparison between spatial and dual-polarized MIMO systems, in terms of channel characteristics and achievable capacity.

The main drawback of the MIMO architecture is that the gain in capacity comes at a cost of increased hardware complexity. Antenna selection is a technique using which we can alleviate this cost. We emphasize that this strategy is all the more relevant for compact devices, which are often constrained by complexity, power and cost. Using theoretical analysis and measurement results, this thesis investigates the performance of antenna selection in dual-polarized MIMO channels. Our results indicate that, antenna selection when combined with dual-polarized antennas, is an effective, low-complexity solution to the problem of realizing higher order MIMO architectures in compact devices.

CHAPTER I

INTRODUCTION

The multiple-input multiple-output (MIMO) architecture has the potential to dramatically improve the performance of wireless systems. MIMO systems increase the spectral efficiency by multiplexing data on parallel independent channels without incurring any cost in terms of bandwidth or power. As a result of this *multiplexing gain*, the capacity of these systems increases linearly with the number of antennas [12]. Furthermore MIMO systems offer additional degrees of diversity which can be used to combat multipath fading in a wireless channel. This leverage, often referred to as the *diversity gain*, reduces the signal fluctuations and improves the overall link reliability [15]. These salient features make MIMO, an indispensable technology for future wireless systems requiring high data rates, such as wireless local area networks (WLANs), broadband wireless access networks (WiMaX) and third and fourth generation cellular networks (3G and 4G).

The multiplexing and diversity gains achieved by a MIMO system are a strong function of the channel characteristics, which in turn depend on the scattering environment and on the array configuration deployed at the transmitter and the receiver [39]. Much of the focus of research has been on uni-polarized spatial array configurations where the multiple antenna elements are separated in space. These systems require an inter-element spacing of the order of a wavelength to achieve significant gains in indoor environments; even larger spacing is required for line-of-sight (LOS) channels [26]. Thus the current trend of miniaturization, seems to be at odds with the implementation of spatial MIMO architectures in portable handheld devices. Also having multiple antennas separated far apart in space could complicate the physical design of devices.

In this regard, polarization diversity has received much attention as an attractive alternative for realizing higher order MIMO architectures in compact devices [39]. Polarization diversity refers to the signaling strategy whereby, information signals are transmitted and

received simultaneously on orthogonally polarized waves. Thus two parallel channels can be created without any requirement of spatial separation. Polarization diversity can be exploited by using the following configurations: (1) an array of dual-polarized elements, and (2) an array of spatially separated orthogonally polarized elements, which will be referred to as the hybrid configuration in this thesis. Dual-polarized antennas provide a compact solution [38], wherein a single antenna element can replace two spatially separated uni-polarized elements. On the other hand, hybrid systems exploit both spatial and polarization diversity.

MIMO channels with polarization diversity cannot be modeled like pure spatial channels, because the subchannels of the MIMO channel matrix are not identically distributed [11]. They differ in terms of average received power, Ricean K factor, cross-polar discrimination (XPD) and correlation properties. The main aim of this thesis is to investigate the performance of MIMO systems employing polarization diversity, in comparison with traditional spatial configurations, taking into account these differences in the channel structure.

Polarization diversity has been studied mostly in the context of outdoor mobile communications (See [48] and the references therein). Indoor wireless channels tend to have significantly different characteristics when compared to outdoor channels [22]. Recently a few indoor channel measurements using dual-polarized or hybrid array configurations have been reported in the literature [51, 31, 34, 23, 49]. In [31] the capacity obtained by hybrid systems is compared with uni-polarized spatial systems, as a function of separation between the transmitter (Tx) and receiver (Rx) arrays. [51] presents LOS and non-line-of-sight (NLOS) measurements at $2, 5$ and 60 GHz in a typical indoor environment. But their data analysis is limited to evaluating average received power and XPD as a function of Tx-Rx separation. 2×2 hybrid and dual-polarized configurations have been studied in [49]. But their analysis is limited to an inter-element spacing of $\lambda/2$ and only to LOS channel conditions. All these measurement campaigns reported in literature are restricted to a fixed array geometry, i.e. they do not take into account the spacing between the antenna elements at the transmitter and receiver. Since the main motivation behind using dual-polarized antennas is to achieve compactness, we note that inter-element spacing should be an important factor, while comparing spatial MIMO with dual-polarized/hybrid systems.

The main drawback of the MIMO architecture is that the gain in capacity comes at a cost of increased hardware complexity in terms of multiple RF chains at the transmitter and receiver. Antenna selection is a technique using which we can alleviate this cost, but still exploit the diversity gain offered by the MIMO architecture [36, 18]. This strategy has been extensively studied in the context of spatial MIMO channels (See [36] and the references therein). We emphasize that this strategy is all the more relevant for compact portable devices, which are often constrained by complexity, power and cost. Hence antenna selection, when combined with dual-polarized antennas, may be a solution that could enable compact systems to exploit the benefits of the MIMO architecture, with only a nominal increase in complexity. Owing to the fact that the channel characteristics of dual-polarized MIMO systems are significantly different from those of spatial channels, the performance of antenna selection needs to be re-evaluated for these systems. To the best of our knowledge, this issue has not been addressed in the literature.

In this thesis, we report on an indoor channel measurement campaign conducted at 2.4 GHz using dual-polarized antennas. We analyze the measured data in terms of the Ricean K factor, subchannel correlations and cross-polar discrimination (XPD). We highlight the differences between vertically polarized and horizontally polarized transmissions in the course of our analysis. In our measurements, we observe a coincidence of low K factors and high XPD values. In such channels, MIMO configurations employing polarization diversity incur a diversity and an SNR loss when compared to spatial configurations. Using the measured capacity distributions, we draw a fair comparison between dual-polarized, hybrid and spatial array configurations. We consider 2×2 and 4×4 MIMO systems for a range of values of inter-element spacing, under LOS and NLOS channel conditions.

In this thesis, we also investigate the performance of antenna selection in dual-polarized MIMO channels. We analytically study the impact of cross-polar discrimination on the achieved selection gain. We first evaluate the performance of the popular capacity based selection strategy [37, 18]. However, capacity based solutions are unlikely to achieve optimum error performance for systems with limited complexity receivers [6]. Hence we analyze

minimum mean squared error (MMSE) based selection for VBLAST (Vertical Bell Labs Layered Space Time Architecture) systems employing linear receivers [14]. Finally, we study the performance of antenna selection for dual-polarized MIMO systems employing orthogonal space time block coding (OSTBC). We provide a theoretical framework for analyzing the performance of norm-based selection for these systems. We use the measured channel samples collected in LOS and NLOS channel conditions, to compare the performance of spatial and dual-polarized MIMO configurations, with respect to antenna selection.

The subsequent portion of the thesis is organized into four chapters. Chapter II makes the reader familiar with the characteristics of the spatial MIMO channel and concept of antenna selection. In the process, it motivates the need for dual-polarized MIMO configurations. Chapter III discusses in detail, the dual-polarized MIMO channel characteristics and their impact on channel capacity. The chapter also presents analytical lower bounds for the ergodic capacity of 2×2 dual-polarized MIMO channels. Chapter IV provides details about the channel measurement campaign and presents data analysis in terms of envelope distributions, subchannel correlations, and XPD. Spatial, dual-polarized and hybrid MIMO configurations are analyzed and compared in terms of achievable capacity in this chapter. Chapter V deals with the problem of antenna selection for dual-polarized MIMO channels. It provides analysis for systems employing VBLAST and OSTBC. Chapter VI concludes the findings of this thesis and presents the scope of extending this work in future. We wish to mention that throughout this thesis, an effort has been made to augment measurement and simulation results with theoretical analysis, wherever possible.

CHAPTER II

BACKGROUND

Multiple input multiple output (MIMO) communication systems employ multiple antennas at the transmitter and the receiver. The input-output relation for a $n_r \times n_t$ narrowband MIMO channel with n_t transmit and n_r receive antennas can be expressed as

$$\mathbf{r} = \sqrt{\frac{E_s}{n_t}}\mathbf{H}\mathbf{s} + \mathbf{n}, \tag{1}$$

where $\mathbf{r}$ and $\mathbf{s}$ are the baseband complex received and transmitted signal vectors respectively. $\mathbf{n}$ represents the circularly symmetric complex Gaussian noise vector with autocorrelation $R_{nn} = \sigma^2\mathbf{I_{n_r}}$. Here, $\mathbf{I_{n_r}}$ is an identity matrix of size $n_r \times n_r$. E_s denotes the total transmit signal power which is equally distributed among all the transmit antennas. $\mathbf{H} = [h_{ij}]$ is $n_r \times n_t$ channel transfer matrix with its entries h_{ij} representing the complex subchannel gain between the jth input and the ith output. We define SNR as $\rho = E_s/N_o$. In this thesis we assume perfect channel knowledge at the Rx but none at the Tx.

Traditionally multiple transmit and receive antennas have been used to combat multipath fading and interference. The *diversity gain* offered by MIMO systems, reduces the signal fluctuations and improves the overall link reliability [15]. The diversity performance of a MIMO channel is dictated by the statistics of its squared Frobenius norm [39], given by

$$W = \|\mathbf{H}\|_F^2 = \sum_{i=1}^{n_r}\sum_{j=1}^{n_t}|h_{i,j}|^2 = \sum_{i=1}^{r}|\lambda_i|^2 \tag{2}$$

where λ_i, $1 \leq i \leq r$ are the r non-zero eigenvalues of the matrix $\mathbf{H}$ and $r \leq \min(n_t, n_r)$ is its rank. Receive diversity techniques like maximal ratio combining (MRC), equal gain combining (EGC) and selection combining (SC), have been popular techniques to leverage this benefit for single-input-multiple-output (SIMO) channels [5]. Recently transmission strategies like space time block coding (STBC), which effectively exploit the diversity gain of MIMO channels, have been proposed in the literature [2, 47].

Multiple receive antennas have also been used to enhance the SNR of the received signal. Coherent combination of the signals impinging on different receive antennas, results in an *array gain* for the system. The average increase in the SNR is proportional to average squared Frobenius norm of the channel, $\bar{W} = E\{\|\mathbf{H}\|_F^2\}$.

A MIMO channel can be decomposed into r parallel non-interfering single-input-single-output (SISO) channels (eigenmodes) with gains $|\lambda_i|^2$, $1 \leq i \leq r$. By multiplexing independent data onto these independent channels, we can get an r-fold increase in spectral efficiency in comparison to a SISO system. This increased data rate is called the *multiplexing gain*. Optimal exploitation of these eigenmodes requires perfect channel knowledge at the Tx. But, suboptimal layered signaling techniques like VBLAST have been proposed [12]. In VBLAST, which is often referred to as spatial multiplexing, the data stream is multiplexed into n_t parallel streams, which are then independently encoded and transmitted using the n_t antennas.

Shannon Capacity is an important measure of performance for communication systems. It indicates the maximum achievable data rate for a given bandwidth and power. We note however, that this metric does not take into account, another important constraint effecting most communication systems, namely complexity. The open loop MIMO capacity for a unit-bandwidth static MIMO channel $\mathbf{H}$, at a reference SNR of ρ, is given by [13]

$$C(\mathbf{H}, \rho) = \log_2 \left[\det \left(\mathbf{I}_{n_r} + \frac{\rho}{n_t} \mathbf{H}\mathbf{H}^H \right) \right], \tag{3}$$

where $\mathbf{A}^H$ denotes the conjugate transpose of the matrix $\mathbf{A}$. Strictly speaking this metric measures the spectral efficiency of the channel. In the presence of fading, $\mathbf{H}$ is a random matrix and $C(\mathbf{H}, \rho)$ is a random variable. The relevant capacity metric for fading channels is the ergodic capacity, which is defined as

$$\begin{aligned} \bar{C}(\rho) = E\{C(\mathbf{H}, \rho)\} &= E\left\{ \log_2 \left[\det \left(\mathbf{I}_{n_r} + \frac{\rho}{n_t} \mathbf{H}\mathbf{H}^H \right) \right] \right\} \\ &= \sum_{i=0}^{r} E\left\{ \log_2 \left(1 + \frac{\rho}{n_t} |\lambda_i|^2 \right) \right\}. \end{aligned} \tag{4}$$

Here $E\{Z\}$ denotes the expectation of the random variable Z. Clearly, the ergodic capacity of a narrowband MIMO channel is a strong function of the channel statistics, especially of

the rank, eigenvalues and the squared Frobenius norm. The statistical nature of the channel is in turn dictated by the array configuration deployed at the Tx and Rx and also by the wireless environment [39].

2.1 Spatial MIMO channels

Much of the focus of MIMO research has been on uni-polarized spatial array configurations where the antenna elements are separated in space. In this thesis, spatial MIMO channels serve as a benchmark, against which the performance of dual-polarized MIMO channels is compared. Shown in Figure 1, is a typical 2×2 spatial MIMO system. Here d measures the physical separation between the antenna elements. Herein, we briefly describe the

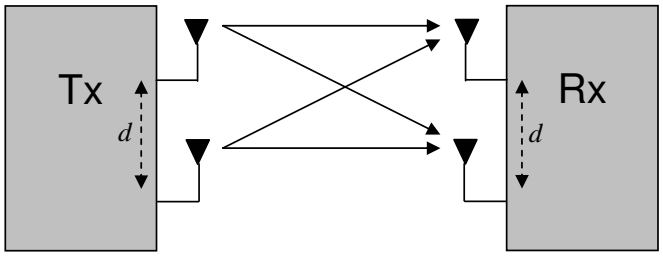

Figure 1: 2×2 MIMO with vertically polarized spatial array configuration

characteristics of a spatial MIMO channel. In the process we highlight the practical difficulties in realizing these structures in compact devices and motivate the use of dual-polarized antennas.

Subchannel powers

All the subchannels of a normalized spatial MIMO channel have unity average power. The average squared Frobenius norm of a spatial channel is given by, $\bar{W} = n_r n_t$ [12, 39]. Thus the spatial MIMO channel achieves maximum possible array gain. Further it can achieve a maximum of $\eta = n_r n_t$ degrees of diversity. The actual diversity gain depends upon the correlation between the subchannels.

Envelope distributions

Under LOS conditions, all the subchannels of a spatial MIMO channel matrix $\mathbf{H}$, have a non-zero mean because of the presence of a direct component. For such channels, the

envelope of the subchannel gains, $R = |h_{ij}|$, is well modeled by a Ricean distribution [43]

$$f_R(r) = \frac{2(K+1)r}{\Omega}\exp(-K - \frac{(K+1)r^2}{\Omega})I_o(2\sqrt{\frac{K(K+1)}{\Omega}}r) \quad r \geq 0, K \geq 0, \Omega \geq 0 \quad (5)$$

where $I_n(.)$ is the n-th order Bessel function of the first kind, $\Omega = E\{R^2\}$ and K is the Ricean factor. The K factor characterizes the Ricean distribution and is the ratio between the average powers of the deterministic and the random components of the channel. In the absence of any dominant paths, $K = 0$ and the Ricean distribution reduces to a Rayleigh distribution given by [43]

$$f_R(r) = \frac{2r\exp(\frac{r^2}{2\Omega})}{\Omega} \quad r \geq 0, \Omega \geq 0. \quad (6)$$

The MIMO channel matrix can thus be decomposed into a LOS and NLOS components as follows [39]

$$\mathbf{H} = \sqrt{\frac{K}{K+1}}\mathbf{H}_{\text{LOS}} + \sqrt{\frac{1}{K+1}}\mathbf{H}_{\text{NLOS}} \quad (7)$$

For i.i.d Rayleigh MIMO channels, the authors in [13] have shown that the ergodic capacity increases linearly with $r = \min(n_r, n_t)$, for a fixed transmit power and bandwidth. This result is the main inspiration for much of the research into MIMO systems. While the linear growth of capacity with the number of antennas is indicative of the tremendous potential of multiple antenna systems, the result is limited in scope by the assumptions it makes. These assumptions hold only in 'ideal' NLOS conditions, where the subchannels of a spatial MIMO channel are uncorrelated. In this case, the spatial channel achieves the maximum diversity order of $\eta = n_r n_t$. However, any correlation between the subchannels reduces the diversity gain [42].

Capacity of Ricean MIMO channels has been studied in [17, 39]. Clearly, $\mathbf{H}_{\text{NLOS}}$ dominates channel behavior for low values of K, while $\mathbf{H}_{\text{LOS}}$ dominates as K increases. When $\mathbf{H}_{\text{LOS}}$ is full rank, the capacity of a MIMO channel increases with K. However in scenarios where $\mathbf{H}_{\text{LOS}}$ is rank-deficient, a high K factor could be a liability. Physically, a rank deficient LOS component results when the separation between the Tx and Rx, $D >> d$. Hence the inter-element spacing should be large for short-range LOS MIMO channels. Traditionally, the elements of $\mathbf{H}_{\text{LOS}}$ have been modeled using the plane-wave assumption. However,

it has been recently shown in [26], that the plane-wave model under-estimates the capacity of short-range LOS spatial MIMO channels. Hence [26] proposes to calculate the elements of the LOS component, precisely based on the inter-element spacing and the separation between the Tx and Rx.

Subchannel correlations

Any correlation between the subchannels diminishes the diversity gain of a MIMO system and thus diminishes its capacity [42]. According to the Kronecker product model [29], under the assumption that all the antenna elements in a MIMO configuration have the same polarization and antenna pattern, the correlation between the elements at the transmitter can be considered independent of the receiver element chosen as the reference and vice versa. The correlation matrix can then be written as

$$\mathbf{R} = \mathbf{\Theta_R} \otimes \mathbf{\Theta_T}, \tag{8}$$

where $\mathbf{\Theta_R} = [\theta_{ij}^R]$ and $\mathbf{\Theta_T} = [\theta_{i,j}^T]$ are the $n_R \times n_R$ and $n_T \times n_T$ correlation matrices on the receive and transmit side respectively. The elements of these Hermitian matrices are given by

$$\begin{aligned} \theta_{i,j}^R &= < h_{i,m}, h_{j,m} > \\ \theta_{i,j}^T &= < h_{m,i}, h_{m,j} >, \end{aligned} \tag{9}$$

where $< a, b >$ is the power correlation coefficient between the complex random variables a and b, defined as [29]

$$< a, b >= \frac{E\left[|a|^2\ |b|^2\right] - E\left[|a|^2\right] E\left[|b|^2\right]}{\sqrt{E\left[|a|^4\ - \left(E\left[|a|^2\right]\right)^2\right] E\left[|b|^4\ - \left(E\left[|b|^2\right]\right)^2\right]}}. \tag{10}$$

We note that the magnitude of the complex correlation can be approximated from the power correlation values as $|\theta_{\text{complex}}| \approx \sqrt{\theta_{\text{power}}}$ [32].

Shown in Figure 2, is the variation of ergodic capacity of a 2×2 Rayleigh MIMO channel as a function of transmit correlation for $\theta^R = 1$, $\rho = 20$ dB. It is evident from the figure that as the correlation between the subchannels increases, the capacity decreases. Correlation between the subchannels is in turn dependent on the multipath richness of the environment

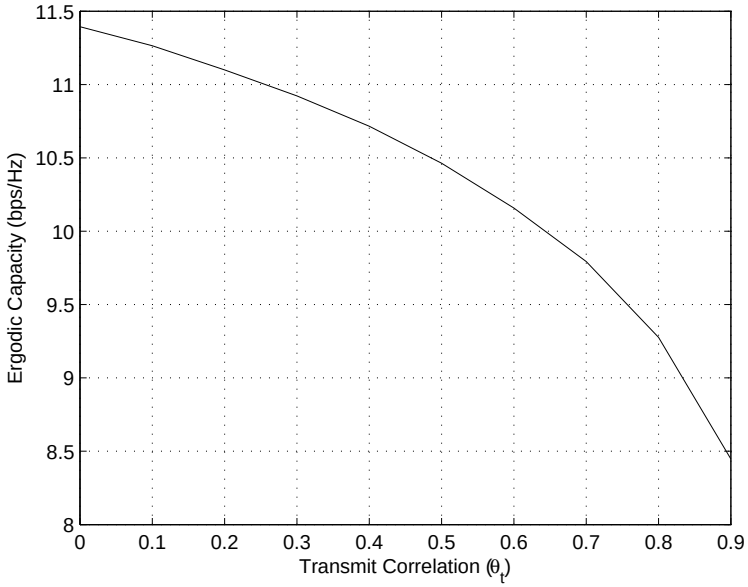

Figure 2: Impact of transmit correlation on the ergodic capacity of a 2×2 Rayleigh MIMO channel with $\theta^R = 0$ and SNR = 20 dB

and on the inter-element spacing between the antenna elements. In general, increasing the inter-element spacing enhances the achievable capacity, especially in scenarios with limited scattering [42, 26].

It is evident from this discussion that the inter-element spacing dictates the performance of spatial MIMO channels, especially in environments with limited scattering, like the LOS channels. A large inter-element spacing is required to lower the subchannel correlations and ensure a full-rank for $\mathbf{H}_{\text{LOS}}$. Typically d needs to be of the order of a wavelength for these channels [26]. When $d < \lambda/2$, the mutual coupling between the adjacent antenna elements results in diminished capacity [24, 35]. Hence a minimum inter-element spacing of $\lambda/2$ is recommended even in NLOS channels. Note that at 2.4 GHz, which is the transmission frequency for indoor WLAN, $\lambda = 12.0$ cm. Thus this requirement of large inter-element spacing, renders the realization of spatial MIMO configurations impractical for many compact devices, especially at lower frequencies.

2.2 Antenna Selection

Implementation of the MIMO architecture requires, in addition to the multiple antennas, complex digital signal processing (DSP) and multiple radio-frequency (RF) chains at the Tx and Rx. Antennas are generally cheaper elements and the additional DSP is becoming less of a burden as digital processing become even more powerful. However, each RF chain consists of hardware units such as analog-to-digital converters, mixers, and low-noise amplifiers, which are extremely expensive and power consuming.

Antenna selection is a technique which can alleviate these costs, but still exploit the diversity benefits offered by the MIMO architecture. This strategy has been extensively studied in the context of spatial MIMO channels. In this section, we provide an overview of antenna selection. We also motivate the use of antenna selection with dual-polarized antennas in compact devices.

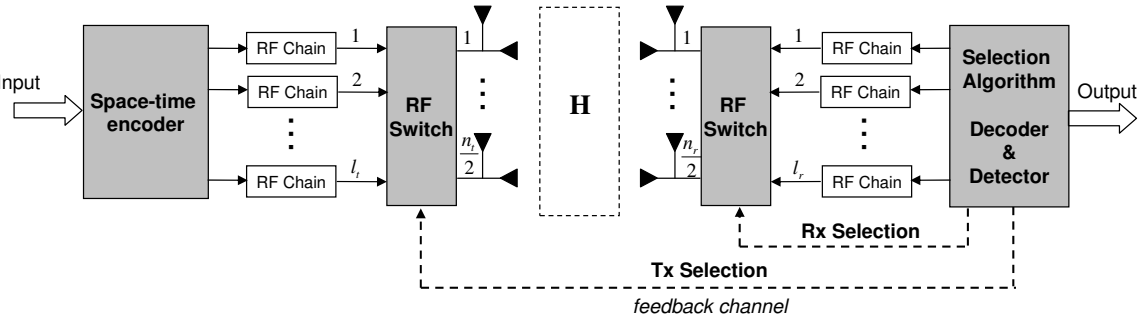

Figure 3: Dual-polarized MIMO with $(n_r, l_r)/(n_t, l_t)$ antenna selection

Given a specific channel realization, a selection algorithm can be implemented in DSP to select the "optimal" l_t out of the n_t available transmit antennas and/or the "optimal" l_r out of the n_r receive antennas. Symbolically we denote this process as $(n_r, l_r)/(n_t, l_t)$ selection. Figure 3 depicts a typical antenna selection system with dual-polarized antennas. This strategy also requires a RF switch at the Tx and Rx.

Implementation of selection at the Tx requires feedback of information from the Rx, as shown in Figure 3. This is an example of a closed-loop MIMO system. In order to maximize the capacity of such a system, the transmitter should distribute its power optimally across the various eigenmodes using water-pouring. Thus to maximize the performance, optimal

power allocation should be implemented in conjunction with antenna selection at the Tx [8]. In this paper we do not address the issue of power allocation. We assume that the selection algorithm is implemented at the receiver and simply the information about the optimal subset of the transmit antennas is fed back through a low bandwidth feedback channel. We note that low bandwidth feedback channels are typically available in many communication systems for synchronization, power control, rate adaptation, and automatic repeat request (ARQ). Thus selection can be easily implemented at the transmitter.

In a typical antenna selection system, the receiver estimates the $n_r \times n_t$ channel matrix $\mathbf{H}$. The l_r available receive RF chains and the l_t available transmit RF chains have to switch through all the antennas, to facilitate channel estimation at the receiver. In this thesis we assume perfect channel knowledge at the receiver. Further, the feedback of selection information to the transmitter incurs a delay. Thus antenna selection is generally suitable for quasi-static channels. In this thesis, we consider block fading channels with Rayleigh or Ricean distributions. We note that adaptive antenna selection strategies for time varying channels have been recently proposed [7].

A typical selection strategy is devised to optimize a certain performance metric, $\mathcal{F}(\bar{\mathbf{H}})$. $\bar{\mathbf{H}}$ is obtained by eliminating $n_r - l_r$ columns and $n_t - l_t$ rows from $\mathbf{H}$ and $S(\bar{\mathbf{H}})$ denotes the set of all possible $\bar{\mathbf{H}}$, whose cardinality is $\binom{n_r}{l_r}\binom{n_t}{l_t}$. The problem reduces to finding the $l_r \times l_t$ submatrix $\widetilde{\mathbf{H}} \in S(\bar{\mathbf{H}})$ that optimizes the function $\mathcal{F}(\bar{\mathbf{H}})$.

Various antenna selection schemes have been studied in the literature. A selection mechanism is proposed in [18], according to which the best subset of transmit and receive antennas is selected to maximize the Shannon capacity. This approach has been very popular and has been extensively studied in the context of spatial MIMO channels (See [37] and the references therein). However, such antenna selection solutions are unlikely to achieve optimum error performance for systems with limited complexity receivers [14]. Hence selection criteria have to be tailored to different receiver implementations. Different approaches to minimize the error rates of spatial multiplexing systems using linear receivers have been proposed in the literature [14, 19, 6]. Also, selection mechanisms to maximize the channel Frobenius norm, have been proposed for MIMO systems employing orthogonal

space time coding (OSTBC) techniques [20, 46].

Selection of the optimal subset of antennas requires an exhaustive search. Although feasible when n_r and n_t are small, it is impractical for higher order MIMO configurations. Hence sub-optimal algorithms have been proposed for the various schemes described above. Efficient algorithms for the capacity maximizing scheme can be found in [21, 41]. For spatial multiplexing systems, sub-optimal algorithms corresponding to the various strategies have been proposed [14, 19, 6]. For space-time coded systems, the selection strategy involves the calculation of the norm which is not very computationally intensive. Hence no algorithms have been proposed for these systems.

Compact devices are often constrained by complexity, cost and power. Hence antenna selection is all the more relevant for these systems. However, as discussed in the previous section, dual-polarized antennas are the only way to realize higher order MIMO architectures in compact devices. To the best of our knowledge, the issue of antenna selection for dual-polarized MIMO channels has not been addressed in the literature.

In this thesis, we study the performance of various antenna selection strategies for dual-polarized MIMO channels. We first analyze the performance of capacity based selection. We then consider MMSE based selection for VBLAST systems and norm based selection for systems employing OSTBC. We use the measured channel samples to a compare the performance of antenna selection for spatial and dual-polarized configurations, in terms of bit-error-rate (BER) and capacity, for a range of values of the array length (L).

CHAPTER III

DUAL-POLARIZED MIMO CHANNELS

The requirement of large inter-element spacing, renders the spatial array configuration impractical for implementing higher order MIMO architectures in compact devices. In this regard, dual-polarized antennas have received much interest as a compact alternative. In this section, we provide a detailed overview of dual-polarized MIMO channels, based upon the insights developed during the course of this research.

3.1 Polarization Diversity

Polarization of an electromagnetic (EM) wave is defined as the direction of its electric field vector. Polarization diversity refers to the transmission strategy whereby, information signals are transmitted and received simultaneously on orthogonally polarized waves. Thus two parallel channels can be created without any requirement of spatial separation. Antennas are referred to as vertically or horizontally polarized, based upon the polarization of the electromagnetic waves they transmit and receive. In practice two polarization schemes are typically used: horizontal/vertical ($0\,^\circ/90\,^\circ$) or slanted ($+45\,^\circ/-45\,^\circ$). In this work we will use the horizontal/vertical configuration.

When an EM wave traveling through air collides with a wall or ceiling, the properties of the reflected waves would depend upon the kind of material the walls or ceiling are made of and also upon the state of polarization of the incident wave. As a result, the propagation characteristics of the vertically and the horizontally polarized waves are significantly different [33]. In the course of this thesis, we attempt to highlight these differences. Further, the transmitted EM wave as it traverses through the wireless channel, undergoes multiple reflections and scattering, resulting in a coupling into the orthogonal state of polarization. This phenomenon is referred to as *depolarization* and is a characteristic property of wireless channels. Depolarization mainly occurs because of oblique reflections of the walls and

scattering from indoor clutter. Thus the extent of depolarization depends on the level of scattering in the environment.

Polarization diversity can be exploited by using the following configurations: (1) an array of dual-polarized elements, and (2) an array of spatially separated orthogonally polarized elements. Dual-polarized antennas provide a compact solution, wherein a single antenna element can replace two spatially separated uni-polarized elements. On the other hand, hybrid systems exploit both spatial and polarization diversity.

Dual-polarized antennas can be visualized as a combination of two co-located antennas ideally with orthogonal polarization. By using a dual-polarized feed, an antenna can transmit two orthogonally polarized waves on the same frequency. Another such antenna can then receive the two orthogonally polarized waves and separate them by means of an electrically identical dual polarized feed. In this thesis, we assume that dual-polarized antennas can perfectly separate vertically and horizontally polarized waves and focus only on the depolarization resulting from the propagation channel.

3.2 System Model

When antennas with different polarizations are used at both ends of a MIMO link, the properties of the channel matrix **H** are significantly different from the uni-polarized spatial case. Shown in Figure 4, is a 2×2 dual-polarized MIMO system. Note that here $d = 0$, which is the main motivation behind using this configuration. Here h^{VV} and h^{HH} denote

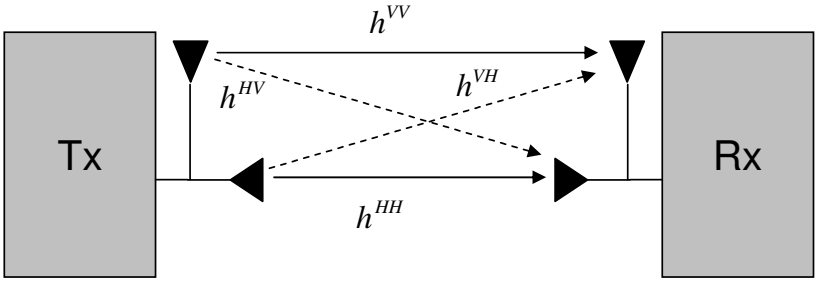

Figure 4: 2×2 MIMO with dual-polarized antennas

the vertically polarized and horizontally polarized co-polar subchannels, while h^{HV} and h^{VH} are the corresponding cross-polar subchannels. For spatial MIMO configurations, all

the subchannels of $\mathbf{H}$ are usually modeled as identically distributed with unity variance. However, when antennas with different polarizations are employed, the properties of the co-polar subchannels differ significantly from those of the cross-polar subchannels. Hence for a $n_r \times n_t$ hybrid and dual-polarized MIMO configurations, the channel matrix can be conveniently written as

$$\mathbf{H} = \begin{bmatrix} \mathbf{H}^{VV}_{(n_r^V \times n_t^V)} & \mathbf{H}^{VH}_{(n_r^V \times n_t^H)} \\ \\ \mathbf{H}^{HV}_{(n_r^H \times n_t^V)} & \mathbf{H}^{HH}_{(n_r^H \times n_t^H)} \end{bmatrix}_{(n_r \times n_t)} \tag{11}$$

Here n_t^V, n_t^H are the number of vertical and horizontally polarized elements at the transmitter respectively. Similarly n_r^V, n_r^H are the number of vertical and horizontally polarized elements at the receiver respectively. When dual-polarized antennas are used at either ends, $n_r^V = n_r^H = n_r/2$ and $n_t^V = n_t^H = n_t/2$. The elements of the submatrices $\mathbf{H}^{VV} = [h_{ij}^{VV}]$ and $\mathbf{H}^{HH} = [h_{ij}^{HH}]$ correspond to the co-polar subchannels in $\mathbf{H}$, while $\mathbf{H}^{VH} = [h_{ij}^{VH}]$ and $\mathbf{H}^{HV} = [h_{ij}^{HV}]$ correspond to the cross-polar subchannels. In the following subsections, we highlight the differences between the subchannels of this MIMO channel matrix.

3.3 Channel Characteristics

In this section we discuss the statistical nature of the channel matrix, $\mathbf{H}$, in the presence of polarization diversity and study their impact on channel capacity.

3.3.1 Subchannel Power Imbalances

In a spatial MIMO channel, the average received power on all the subchannels is identical. However this is not true for the case of MIMO channels with polarization diversity. We consider a 2×2 MIMO system using a dual-polarized antenna at both ends, to study these power imbalances between the various subchannels. The channel matrix in (11) reduces to:

$$\mathbf{H} = \begin{bmatrix} h^{VV} & h^{VH} \\ h^{HV} & h^{HH} \end{bmatrix}, \tag{12}$$

The cross-polar subchannels of the channel matrix result from the depolarization of the transmitted signal. The average power of these subchannels depends on the cross-polar

discrimination (XPD) of the channel. XPD measures the extent of depolarization in a wireless channel and is defined as [27]

$$\begin{aligned} X_V &= E\{|h^{VV}|^2\}/E\{|h^{HV}|^2\} \\ X_H &= E\{|h^{HH}|^2\}/E\{|h^{VH}|^2\} \end{aligned} \tag{13}$$

Implicit in these definitions, is the assumptions that the XPD of the dual-polarized antennas is infinity, i.e. there is perfect isolation between the orthogonal feeds. Most authors assume that $X_V \approx X_H$, but we note that this is not always true owing to the fact that depolarization not only depends on the environment, but also on the antenna patterns of the V and H elements [51]. In general, high values of XPD would indicate a higher level of separability between the two states of polarization and such channels are amenable to polarization multiplexing techniques. On the other hand channels with lower values of XPD would indicate significant cross-coupling between the two states of polarization and encourage diversity techniques [38]. Under LOS channel conditions where the K factor is high, a high XPD could help diagonalize an otherwise rank deficient spatial MIMO channel. However in NLOS scenarios, a high XPD would indicate a diversity deficit for MIMO systems employing polarization diversity when compared to traditional spatial configurations.

The propagation characteristics of the vertically and the horizontally polarized waves are significantly different. In general $E\{|h_{VV}|^2\} > E\{|h_{HH}|^2\} = \beta \leq 1$, because of the Brewster angle phenomenon for horizontally polarized transmission [33]. This disparity could also arise from the differences in the antenna patterns of the orthogonally polarized elements.

Taking into account these subchannel power losses, the average squared Frobenius norm of this channel can be written as

$$\bar{W} = n_r^V n_t^V + \beta(n_r^H n_t^H) + \frac{1}{X_V}(n_r^H n_t^V) + \frac{\beta}{X_H}(n_r^V n_t^H) \leq n_r n_t. \tag{14}$$

Note that as XPD increases or as β increases, $\bar{W}$ diminishes. As a result, the array gain achieved by using multiple dual-polarized antennas is smaller when compared to pure spatial channels. Also due to these power losses, the diversity gain of a dual-polarized MIMO channels is diminished for high XPD, β values. For example, the available degrees of

diversity for a $(n_r \times n_t)$ i.i.d. Rayleigh MIMO channel are $\eta_s = n_r \cdot n_t$ [39]. But for dual-polarized NLOS channels with $\beta = 1$ and $X_V = X_H = X \to \infty$, the number of diversity orders offered by the channel are

$$\eta \approx n_r^V n_t^V + n_r^H n_t^H < n_r n_t. \tag{15}$$

Thus MIMO systems employing polarization diversity incur SNR and diversity penalties, when compared to their spatial counterparts.

3.3.2 Envelope Distributions

In a LOS scenario, it is well known that the envelope of the co-polar subchannels $(h_{ij}^{VV}, h_{ij}^{HH})$, follow a Ricean distribution (5). However, it is important to note that even in LOS conditions, the cross-polar subchannels $(h_{ij}^{VH}, h_{ij}^{HV})$, follow a Rayleigh distribution [11]. This can be attributed to the fact that when we have orthogonally polarized antennas with good isolation properties, at both ends of the link, the cross-polar terms are completely because of diffuse scattering and hence the deterministic component of these subchannels is very small. The Rayleigh characteristic is confirmed by our measurements, as shown in the next chapter. We however point to the possibility of K factors of cross-polar terms being greater than zero for channels with a stationary environment or when the cross-polar discrimination of the antennas is not very good. Under NLOS channel conditions, the K factor for both co-polar and cross-polar subchannels is 0 and hence all the subchannels follow a Rayleigh distribution.

In all when the dual-polarized antennas have high XPD, we can model the cross-polar subchannels as:

$$h_{ij}^{II} = \beta_I \left(\sqrt{\frac{K_{II}}{K_{II}+1}} \bar{h}_{ij}^{II} + \sqrt{\frac{1}{K_{II}+1}} \tilde{h}_{ij}^{II} \right), \tag{16}$$

where, $I \in \{V, H\}$ and $\beta_V = 1$. $\bar{h}_{ij}^{II}$ is a complex number with unit amplitude and a random phase. We can model the phase of $\bar{h}_{ij}^{II}$ according to the spherical wave model [26]. $\tilde{h}_{ij}^{II}$ is a complex random variable with its real and imaginary components following a Normal distribution with zero mean and variance 1/2. The cross-polar subchannels can be modeled

as,

$$h_{ij}^{IJ} = \frac{\beta_J}{X_J}\left(\sqrt{\frac{K_{IJ}}{K_{IJ}+1}}\bar{h}_{ij}^{IJ} + \sqrt{\frac{1}{K_{IJ}+1}}\tilde{h}_{ij}^{IJ}\right), \tag{17}$$

where, $I, J \in \{V, H\}, I \neq J$. $\bar{h}_{ij}^{IJ}$ and $\tilde{h}_{ij}^{II}$ have similar definitions as their co-polar counterparts. We note that for low K factors, the deterministic component in (17) vanishes.

3.3.3 Subchannel Correlations

For MIMO channels employing polarization diversity, owing to the fact that horizontally and vertically polarized antennas have different radiation patters and because the propagation characteristics of vertically polarized waves differ from those of horizontally polarized waves, the Kronecker product model for correlations, is not valid for these systems. The Kronecker model still applies for the co-polar submatrices $\mathbf{H}^{VV}$ and $\mathbf{H}^{HH}$, but not for the cross-polar submatrices $\mathbf{H}^{VH}$ and $\mathbf{H}^{HV}$. For a detailed discussion of correlation modeling for dual-polarized MIMO, we refer the interested reader to [28].

Polarization diversity results in low values of correlations between the subchannels, even in environments where the spatial channels are highly correlated. This is confirmed by our measurement results, presented in the next chapter.

3.4 Channel Capacity

MIMO channels with polarization diversity achieve low correlation between the subchannels, which is beneficial for its capacity, as observed in Figure 2. However, these channels incur SNR and diversity losses which are detrimental to their performance. In this section, we analyze the effect of these power losses on the channel capacity. We also derive an analytical lower bound for the ergodic capacity of 2×2 dual-polarized MIMO channel.

3.4.1 Impact of Subchannel Power Losses

To analyze the impact of these subchannel power losses on the capacity, we consider a 2×2 MIMO channel with a Ricean fading distribution. We assume that $\beta = 1$, $X_V = X_H$ and $K_{VV} = K_{HH} = K$. Further we assume that the subchannels are independent. In Figure 5, we plot the ergodic capacity as a function of XPD for $K \in \{0, 2, 4, 10\}$. It is evident that as the XPD increases, the capacity decreases for both Rayleigh and Ricean

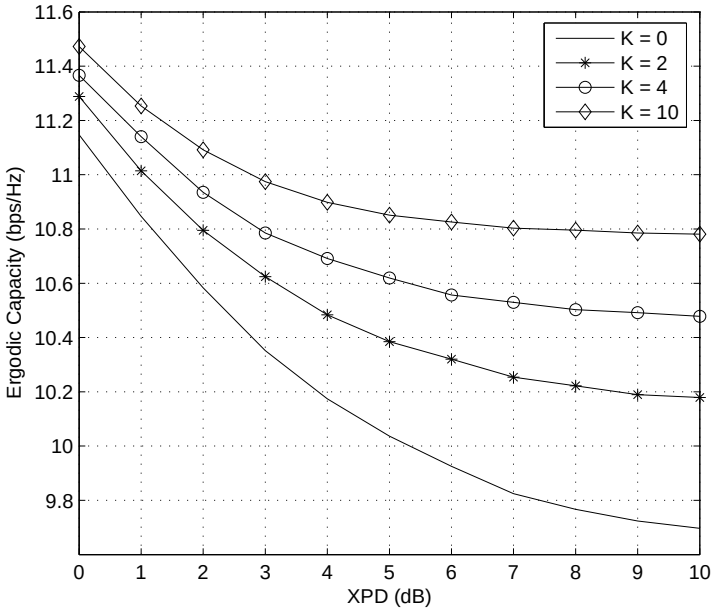

Figure 5: Effect of XPD on the capacity of 2×2 dual-polarized MIMO channels

fading distributions. An interesting observation from Figure 5 is that the capacity decrease is more prominent for lower values of K than for channels with high K factors. This is because, for channels with low K factors, subchannel power losses incur a diversity loss in addition to the SNR loss.

So far, we have discussed how a high XPD value diminishes the capacity of dual-polarized/hybrid MIMO channels. However, there is scenario where a high XPD could help achieve better capacity for dual-polarized MIMO channels, when compared to its spatial channels. Consider a LOS channel with $K \rightarrow \infty$. Further assume a rank deficient 2×2 spatial MIMO channel, which occurs when $d << D$ as discussed in Section 2.1. As a result of this rank deficiency, this channel performs only as good as a SISO link. However, as shown in Figure 6, when we use polarization diversity in such scenarios, the high XPD helps diagonalize the channel matrix. As a result, the dual-polarized configuration can perform better than very compact spatial configurations, in LOS channels.

On one hand, the subchannel power losses are, in general, detrimental to the capacity of MIMO channels employing polarization diversity. But on the other hand, these configurations achieve very low correlation between the subchannels, which is beneficial. Thus

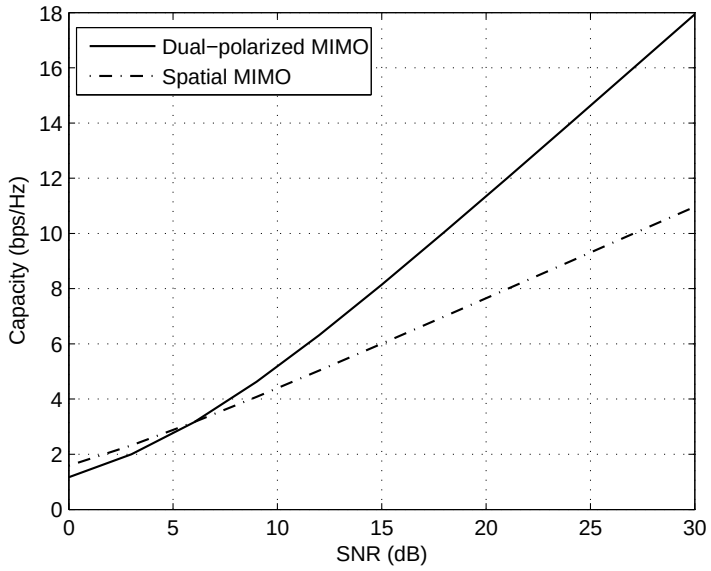

Figure 6: Performance improvement by using polarization diversity in scenarios where the spatial channel is rank deficient. $K \to \infty$ and $XPD \to \infty$

both these conflicting factors have to be taken into account, when evaluating the capacity of MIMO channels in the presence of polarization diversity.

Limiting case: XPD $\to \infty$

Before we conclude this section, we note a few interesting observations about MIMO channels with infinite XPD. Consider a $n_r \times n_t$ MIMO channel with the same assumptions as above. Further assume a dual-polarized configuration where $n_r^V = n_r^H = n_r/2$ and $n_t^V = n_t^H = n_t/2$. In the limiting case of $X_V = X_H = X \to \infty$, the MIMO channel matrix in (11) reduces to

$$\mathbf{H} = \begin{bmatrix} \mathbf{H}^{VV}_{(n_r^V \times n_t^V)} & \mathbf{0}_{(n_r^V \times n_t^H)} \\ \\ \mathbf{0}_{(n_r^H \times n_t^V)} & \mathbf{H}^{HH}_{(n_r^H \times n_t^H)} \end{bmatrix}. \tag{18}$$

Noting that $\det(\mathbf{H}) = \det(\mathbf{H}^{VV}) \cdot \det(\mathbf{H}^{HH})$, we can write

$$C(\mathbf{H}, \rho) = C\big(\mathbf{H}^{VV}, \rho/2\big) + C\big(\mathbf{H}^{HH}, \rho/2\big). \tag{19}$$

This equation implies that in the limiting case, dual-polarized MIMO channel reduces to two non-interfering lower dimensional spatial MIMO channels, one of which is vertically

polarized, while the other is horizontally polarized. This idea has inspired combined multiplexing/STBC based transmission techniques [10].

Further, from (18), we claim that unless $n_r^V = n_t^V$ and $n_r^H = n_t^H$, the MIMO channel matrix is always rank deficient. This claim of ours can be easily proved through contradiction. Hence it is recommended to have equal number of vertically and horizontally polarized elements at the Tx and the Rx.

3.4.2 Analytical Lower Bound for Ergodic Capacity of 2×2 MIMO Channels

For a spatial MIMO channel, all the elements of $\mathbf{H}$ are identically distributed and as a result $\mathbf{W} = \mathbf{H}\mathbf{H}^H$ is a Wishart matrix. Using the properties of these matrices, analytical expressions for ergodic capacity have been derived in the literature [13]. However for dual-polarized MIMO channels, $\mathbf{W}$ is not a Wishart matrix and it is not straightforward to derive exact expressions for ergodic capacity. To the best of our knowledge, [40] is the only paper in the literature that addresses this issue. In this paper, the authors derive lower bounds for 2×2 dual-polarized MIMO, assuming a general physical scattering model.

In this section, we derive tight lower bounds for 2×2 dual-polarized MIMO channels for Ricean and Rayleigh fading distributions. We follow a same approach as [40], but we extend the results therein to derive explicit expressions for the lower bound in terms of Ricean K factor, and the subchannel power losses (XPD, β). The 2×2 dual-polarized MIMO channel matrix can be written as

$$\mathbf{H} = \begin{bmatrix} h^{VV} & h^{VH} \\ h^{HV} & h^{HH} \end{bmatrix}.$$

The correlation between the elements of a dual-polarized MIMO channel is very low. Thus it is reasonable to assume that all the channel entries are independent of each other. Further, we make the simplifying assumption that $X_V = X_H = 1/\alpha$, $0 < \alpha \leq 1$. All the channel entries are assumed to be complex circularly symmetric Gaussian random variables with the following variances

$$\begin{aligned} E\{|h^{VV}|^2\} &= 1; \quad E\{|h_{HH}|^2\} = \beta \\ E\{|h_{HV}|^2\} &= \alpha; \quad E\{|h_{VH}|^2\} = \beta\alpha. \end{aligned} \tag{20}$$

The average power of h^{HH} subchannel is lower than that of h^{VV} because of the Brewster angle phenomenon for horizontally polarized waves as mentioned in the previous section. In general $\alpha \leq \beta \leq 1$. In a LOS scenario, the cross-polar subchannels in $\mathbf{H}$ are Rayleigh distributed while the co-polar subchannels are Ricean distributed. To simplify analysis, we assume that the K factors for both the co-polar subchannels are equal i.e. $K_{VV} = K_{HH} = K$. Thus the cross-polar subchannels have zero mean, while the co-polar subchannels have a non-zero mean given by

$$\begin{aligned} E\{h^{VV}\} &= \sqrt{\tfrac{K}{K+1}} \\ E\{h^{HH}\} &= \sqrt{\tfrac{\beta K}{K+1}}. \end{aligned} \tag{21}$$

Denoting $D = E\{\det\left(\mathbf{I}_2 + \frac{\rho}{2}\mathbf{W}\right)\}$, the expression for ergodic capacity in (3) can be expanded in Taylor series about $E\{D\}$. Ignoring the higher order terms in the expansion, we can arrive at the following lower bound for the ergodic capacity,

$$\bar{C}(\rho) \geq \log_2(E\{D\}) - \frac{\log_2(e)}{2}\frac{E\{D^2\} - (E\{D\})^2}{(E\{D\})^2} \tag{22}$$

To derive a closed form expression for this bound, we need to evaluate $E\{D\}$ and $E\{D^2\}$. $E\{D\}$, which also represents an upper bound to ergodic capacity by Jensens' Inequality, can be derived to be

$$E\{D\} = 1 + \frac{\rho}{2}(1+\alpha)(1+\beta) + \frac{\rho^2}{4}\beta(1+\alpha^2), \tag{23}$$

where w_{ij}, $i,j \in \{1,2\}$ are the elements of the matrix $\mathbf{W}$. Note that the upper bound is not a function of K. Now $E(D^2)$ can be computed to be

$$\begin{aligned} E\{D^2\} &= 1 + \rho(1+\alpha)(1+\beta) \\ &\quad + \frac{\rho^2}{2}(2(1+\alpha^2+\alpha)(1+\beta)^2 + \bar{K}(1+\beta^2)) \\ &\quad + \frac{\rho^3}{4}\beta(1+\beta)((1+\alpha)(2\alpha^2-\alpha+2) + \bar{K}) \\ &\quad + \frac{\rho^4}{16}\beta^2((\bar{K}+2)^2 + 4\alpha^2 + 4\alpha^4), \end{aligned} \tag{24}$$

where $\bar{K} = -K^2/(K+1)^2$. For complete derivations, we refer the interested reader to the Appendix A.

Figure 7 shows the simulated ergodic capacity, obtained through Monte Carlo simulations, and the analytical lower bounds for 2×2 Ricean MIMO channels with $K \in \{0, 1, 10\}$.

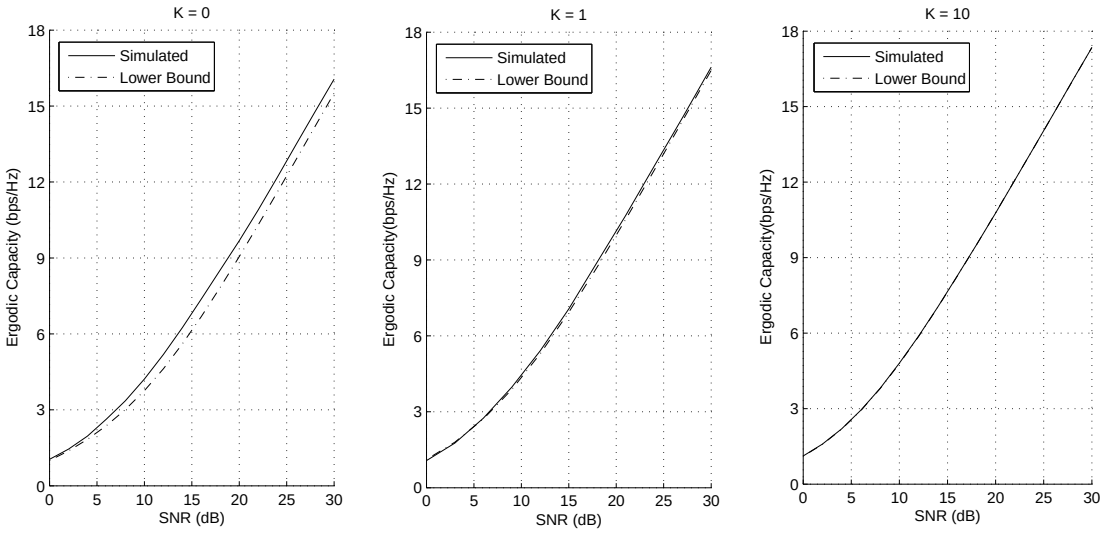

Figure 7: Comparison of the simulated ergodic capacity and the analytical lower bound, for 2×2 MIMO with polarization diversity

The XPD = 10 dB is kept the same for all the three channels. It is clearly seen that the analytical lower bound is a close approximation to the ergodic capacity for both Rayleigh ($K = 0$) and Ricean channels. Further, we can observe that the bound gets tighter as the K factor increases. Infact, for $K = 10$, the bound is almost exact.

To further validate the derived analytical lower bound, in Figure 3.4.2, we compare the measured ergodic capacities under LOS and NLOS channel conditions, with the values predicted by (22). Details of the measurement campaign are provided in the next chapter. In the measured channels $X_V \neq X_H$ and $K_{VV} \neq K_{HH}$. Hence for the predictions, we have used the average of these values. It is evident that the analytical bound provides a close approximation to the measured capacity, under both LOS and NLOS channel conditions. As expected, the bound is tighter for the LOS channel.

Finally we note that the analytical lower bound provides a tight approximation to the ergodic capacity of 2×2 MIMO channels employing polarization diversity, under both Rayleigh and Ricean fading environments and for a range of values of the SNR.

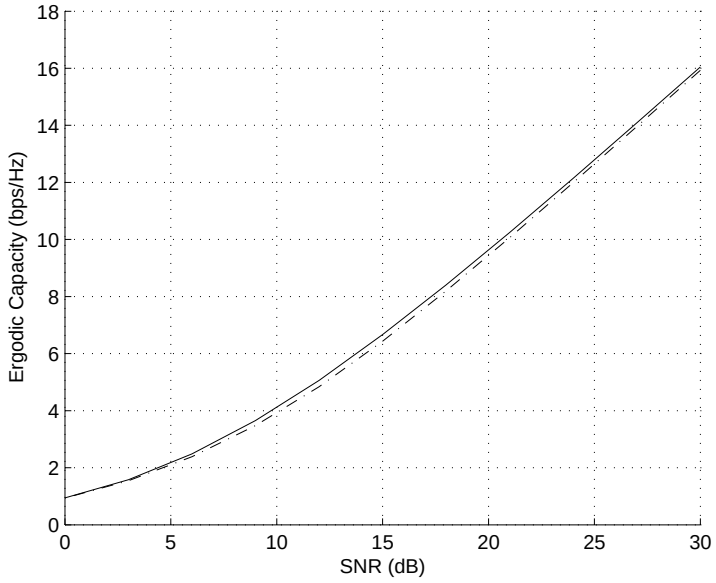

(a)

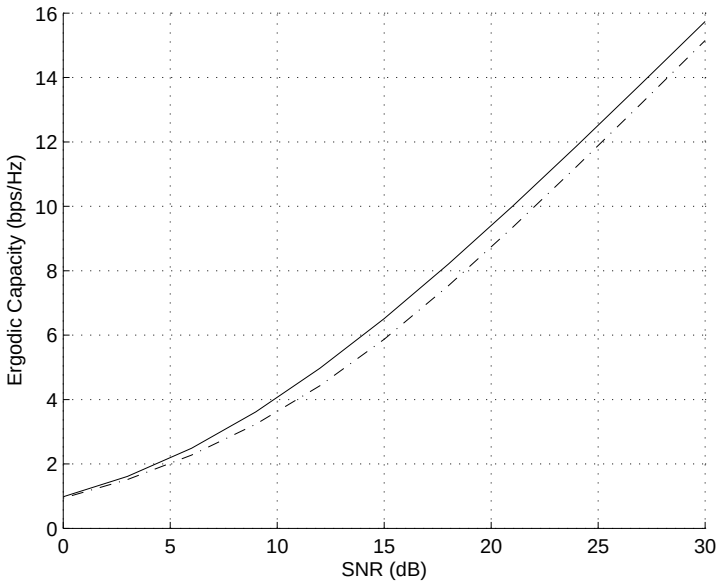

(b)

Figure 8: Comparison of the measured ergodic capacity and the analytical lower bound, for 2×2 dual-polarized under (a) LOS and (b) NLOS channel conditions

CHAPTER IV

MEASURED INDOOR MIMO CHANNELS WITH POLARIZATION DIVERSITY

In this chapter we report on an indoor channel measurement campaign conducted at 2.4 GHz using dual-polarized antennas. We first provide details about the MIMO channel sounding system and about the location where the measurements were taken. We then analyze the measurement data in terms of average power, XPD, Ricean K factor, and subchannel correlations. We highlight the differences between vertically polarized and horizontally polarized transmissions, in the course of our analysis. Using the measured capacity distributions, we draw a fair comparison between dual-polarized, hybrid and spatial array configurations, in terms of achievable capacity.

4.1 Measurement System

The MIMO-channel measurement system used is illustrated in Figure 9. It is composed of two parts: (1) the HP 85301B stepped-frequency antenna pattern measurement system, which, because of its coherent reference signal, can measure the channel frequency response

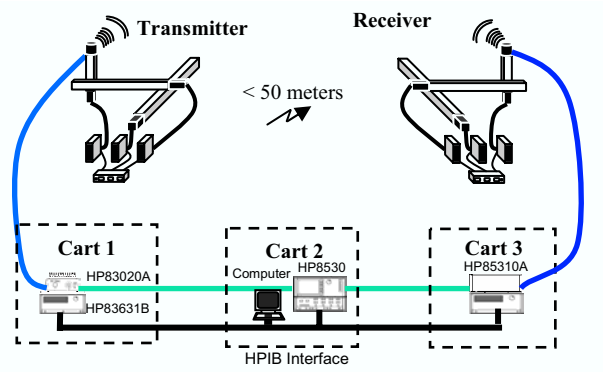

Figure 9: Overview of our virtual array MIMO measurement system. The lower section represents the HP85301B antenna pattern measurement system, and the upper section is the 3D actuator system.

directly, and (2) the actuator positioning system, which creates the virtual array by moving the antenna to arbitrary pre-programmed locations. Figure 10 shows one of the portable platforms and one of the actuator positioning systems. There were two of the setups shown in Figure 10, one for each end of the MIMO link. This measurement system was developed as part of some previous research at the Smart Antennas Research Laboratory (SARL) [25]. This virtual array approach has been validated in [25] and offers great flexibility to experiment with different antenna configurations. But it requires the environment to be kept still throughout the measurement process. For a detailed description of this measurement system, we refer the interested reader to [25].

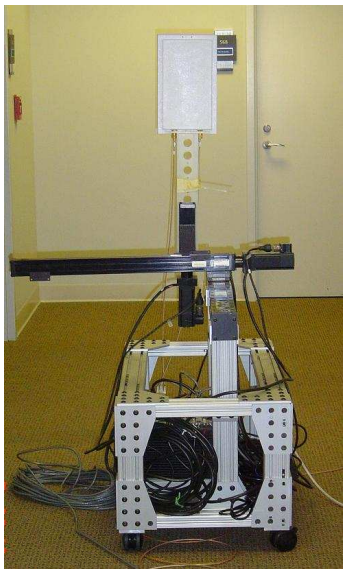

Figure 10: Dual-polarized antenna mounted on the actuator system

The antennas used at both ends are dual-polarized narrowband antennas with a frequency range of 2.400 - 2.483 GHz (model number: SPDPG-4O-H2O, Superpass Company Inc.). The vertical and horizontally polarized elements have omni-directional patterns in the azimuth plane but differ in their elevation patterns [1]. A multi-channel controller HP 85330 and HP 85332 PIN switches are incorporated into the measurement system to measure the co-polar (VV and HH) and the cross-polar (VH and HV) subchannels successively. This automated the entire experiment and reduced the experiment duration by a factor of

[1] http://www.superpass.com/SPDPG-4O-H2O.html

four. The transmitter and the receiver are kept at a height of 1.35 m.

The entire measurement system was integrated, calibrated and tested for repeatability before the actual measurements.

Measurement Settings

A measurement plan was devised, so as to measure MIMO channels for different inter-element spacing (d) values, ranging between $\lambda/2$ to 2λ . A virtual 50 element ($5 \times 5 \times 2$) cubicle array with a minimum inter-element spacing of $\lambda/2$, as shown in Figure 11, is used at the transmitter (Tx) and the receiver (Rx). Previous measurements in the same environment had indicated that the coherence bandwidth of the channel is about 15MHz. Hence corresponding to each pair of transmit and receive antenna locations, six uncorrelated channel samples are used, out of the 64 samples collected in the frequency range of operation.

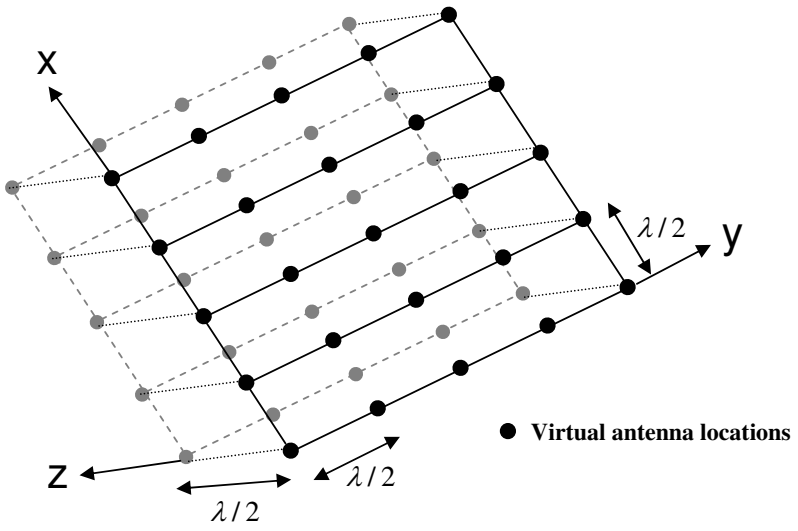

Figure 11: $5 \times 5 \times 2$ Virtual array used for measurements

In order to obtain MIMO channel samples, subarrays of the required size are extracted from the Tx and Rx cubicle arrays. The number of spatial samples depend on the array length (L). In addition to these spatial samples, we also use the frequency samples. In this thesis we consider 2×2 and 4×4 MIMO architectures. Higher order configurations could be analyzed with these measurement settings but we limit our analysis to these configurations,

because the main motivation for this work is compactness. We consider spatial (S), dual-polarized (D) and hybrid (H) array configurations. The number of available samples for each of these configurations is listed in Table 4.1.

Table 1: The number of measured MIMO channel samples (N) for different array configurations

	d	0	$\lambda/2$	λ	$3\lambda/2$	2λ
Spatial/Hybrid	2×2	-	9600	5400	2400	600
	4×4	-	2400	-	-	-
Dual-polarized	2×2	15000	-	-	-	-
	4×4	-	9600	5400	2400	600

Measurement Location

The measurement campaign was conducted on the fifth floor of the Georgia Centers for Advanced Telecommunication Technologies (GCATT) building in Atlanta, GA. The floor plan of the measurement location is illustrated in Figure 12. The walls of the building

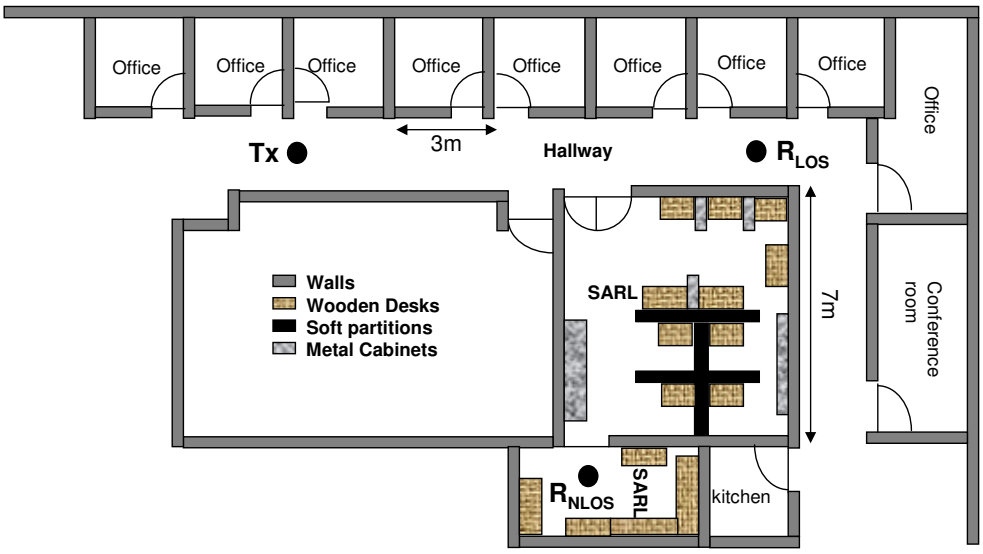

Figure 12: Floor plan of the measurement location

are made of plasterboard with metal-studs in them. The ceiling and the floor are made of reinforced concrete. The LOS measurements were taken in the hallway on the fifth floor,

which is lined by offices on one side and laboratories on the other as shown in Figure 12. The distance between the transmitter and the receiver was approximately 14 m in the LOS scenario. For the NLOS measurements the receiver array was moved into the rear room of the adjoining laboratory and both the doors leading to it were closed.

4.2 Channel Characterization

Using the measured data, we characterize the MIMO channels employing polarization diversity, in terms of average received power, XPD, envelope distributions, and subchannel correlations.

4.2.1 Average power and XPD

Based upon the co-polar and cross-polar subchannel measurements, we evaluate the instantaneous received power for the various subchannels. It can be observed from Figure 13 that in LOS conditions, the instantaneous received power is significantly higher for the co-polar subchannels when compared to the cross-polar subchannels. This is because of the presence

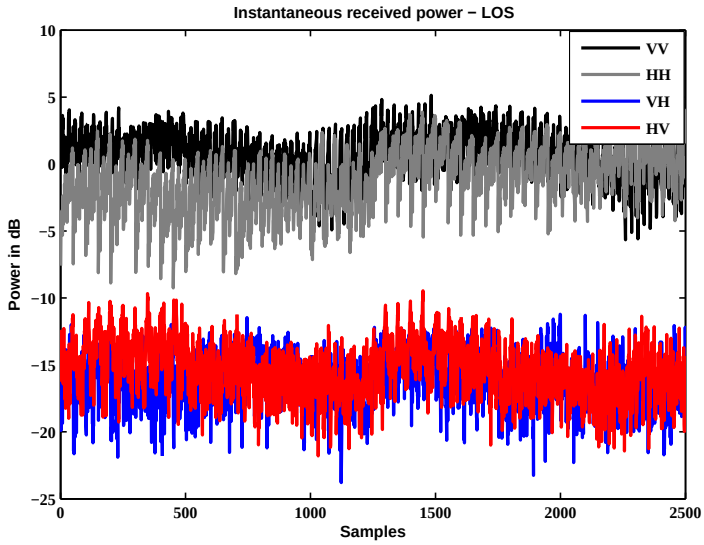

Figure 13: Instantaneous received power on cross-polar and co-polar subchannels under LOS conditions

of a dominant direct component, which results in very little cross-coupling between the orthogonal states of polarization. Thus the XPD values in the LOS scenario are very high.

Such high values of XPD are expected in LOS scenarios [31, 51]. Further, it is also observed that the average received power on VV co-polar subchannel is 1.6 dB higher than the HH subchannel. This can be attributed to the Brewster angle phenomenon [31] for horizontally polarized waves and the difference in the antenna patterns.

In the NLOS environment, as expected the received power on all four channels is significantly lower than the corresponding powers in the LOS case. The average power of the VV co-polar subchannel is 2.2 dB higher than the HH subchannel. Further the difference between the received powers on the co-polar and cross-polar channels is diminished. This is because of an increase in depolarization, when compared to the LOS scenario. However, as shown in Table 2, the XPD values in our NLOS scenario are not as low as the XPD values reported in [31], but values comparable to ours have been reported in [51].

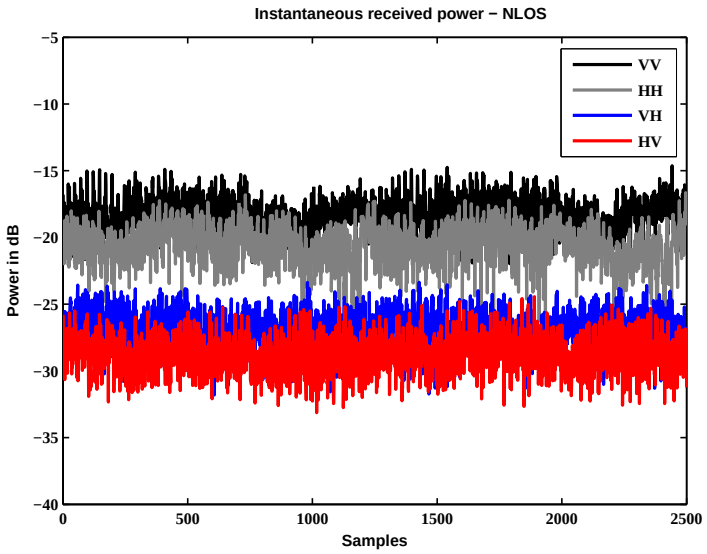

Figure 14: Instantaneous received power on cross-polar and co-polar subchannels under NLOS conditions

Further we have observed that $X_V \neq X_H$ owing to the different propagation characteristics of vertically polarized waves and horizontally polarized waves [31]. This could also result from the difference in the antenna patterns for the vertically polarized and horizontally polarized elements . The difference is significant at 2.5 dB for the LOS scenario, but it is negligible for the NLOS case.

Table 2: Measured XPD values in dB

	X_V	X_H
LOS	16.96	14.50
NLOS	8.58	8.29

In all we conclude that because of the high XPD and β values, under LOS as well as NLOS conditions, the subchannel power losses are significant in our measured channels.

4.2.2 Ricean K factor

Using the measured data, we also evaluate the envelope distributions for the various subchannels. The K factors for the co-polar and cross-polar subchannels were computed using the distribution fitting tool available in MATLAB. Under LOS channel conditions, as shown in Figure 15, it is observed that the co-polar subchannels follow a Ricean distribution, whereas the cross-polar subchannels follow a Rayleigh distribution. This is expected because of the fact that the cross-polar subchannel gains result from depolarization of the transmitted signal, which in turn is because of scattering and oblique reflections. Thus the subchannels of a MIMO channel employing polarization diversity are not identically distributed.

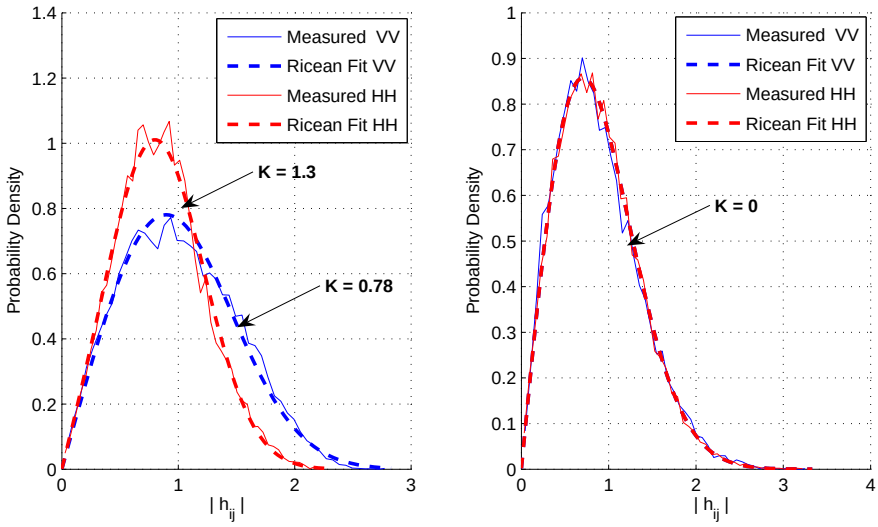

Figure 15: Measured PDFs of the envelopes of: a) co-polar subchannels b) cross-polar subchannels in the LOS scenario

In the hallway, the measured K-factors are 0.78 and 1.30 for VV and HH co-polar subchannels respectively. We note that the moment based estimation method [1], also yields similar values. Although counterintuitive, such low K-factors have been observed in previous measurements in the hallway environment [45], and have been explained based upon the electromagnetic properties of waveguides [30]. Under NLOS channel conditions, as expected, all the subchannels follow a Rayleigh distribution.

4.2.3 Subchannel correlations

The subchannel correlations effect the diversity performance of a MIMO channel as discussed in Section 2.1. They depend on the scattering environment and the antenna configuration deployed at the transmitter and receiver. In this section we evaluate the subchannel correlations, for the measured spatial and dual-polarized/hybrid MIMO channels

For a spatial MIMO channel, subchannel correlations are a strong function of the inter-element spacing at the transmitter and receiver. In order to analyze the impact of inter-element spacing on correlation, we consider a 2×2 uni-polarized spatial MIMO configuration. The spacing between the elements at the transmitter and the receiver is kept the same. We consider both vertically polarized (V) and horizontally polarized (H) configurations. For the measured spatial channels, we have verified that the Kronecker product model, discussed in Section 2.1, is valid. As a result, the correlation statistics of the 2×2 spatial MIMO channel can be analyzed in terms of two parameters: transmit correlation (θ^T) and receive correlation (θ^R), as defined in (9). Shown in Figure 16, is the measured transmit and receive correlation values, for LOS and NLOS channel conditions, as a function of the inter-element spacing.

The general trend suggests that increasing the spacing between the elements decorrelates the subchannels. An inter-element spacing of $d = 3\lambda/2$ is required to sufficiently decorrelate the subchannels in the LOS scenario and any further increase does not significantly decrease the correlation. As expected for NLOS scenarios, correlation values are significantly lower than their corresponding values in LOS. Although a definitive trend can be observed for transmit correlation in the NLOS scenario, there is no trend in the receive correlation values.

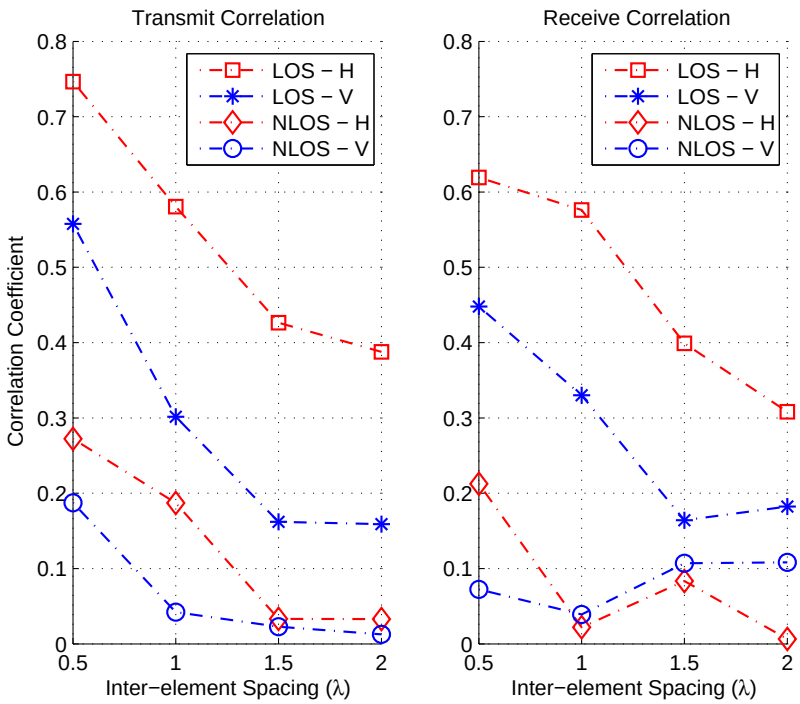

Figure 16: Transmit and receive correlation in LOS and NLOS scenarios

This is because the transmitter is placed in the hallway, whereas the receiver is kept inside an adjoining laboratory, where the angular spread is uniform.

We also note that the horizontally polarized spatial configuration achieves higher correlation values when compared to its vertically polarized counterpart, for both LOS and NLOS scenarios. This could be attributed to the Brewster angle phenomenon, which results in a more narrow angular spread for horizontally polarized waves when compared to vertically polarized waves. Hence owing to the higher correlation values and the loss of power, there is no motivation to use horizontally polarized spatial MIMO configurations.

As noted above, increasing the inter-element spacing can improve the capacity of spatial MIMO channels in LOS scenarios. However, this would lead to impractical form factors for portable devices. Hence a natural alternative would be to use dual-polarized configurations, which could use the additional dimension of polarization to sufficiently decorrelate the channel, even for small inter-element spacing.

The measured dual-polarized/hybrid MIMO channels confirm that the the Kronecker

Table 3: Measured transmit and receive power correlation values for 2×2 vertically polarized spatial MIMO channels

	L	$\lambda/2$	λ	$3\lambda/2$
LOS	θ^T	0.56	0.30	0.18
	θ^R	0.45	0.32	0.18
NLOS	θ^T	0.19	0.05	0.02
	θ^R	0.08	0.04	0.10

model (8) is not valid for these configurations [28]. We have calculated the correlation matrix $\mathbf{R}$, for dual-polarized and hybrid configurations, for $d \in \{0, \lambda/2, \lambda, 3\lambda/2, 2\lambda\}$. The correlation values for these configurations were found to be significantly lower than their spatial counterparts, and were upper bounded by 0.25 in LOS and 0.15 in NLOS scenarios. Further, no definitive trend has been observed, as the spacing between the V and H elements was increased.

Thus a dual-polarized configuration with co-located antennas, is sufficient to achieve low correlation values, even in LOS scenarios.

4.3 Capacity Analysis

In this section we compare the capacity achieved by dual-polarized/hybrid configurations with spatial systems, for different values of inter-element spacing. We consider 2×2 and 4×4 MIMO configurations. On one hand, polarization diversity helps in dramatically reducing subchannel correlations for compact configurations in LOS scenarios. But on the other hand, these systems suffer from subchannel power losses because of high XPD and horizontally polarized transmissions. These subchannel power losses imply diminished degrees of diversity and SNR for MIMO channels with polarization diversity. Thus both these opposing aspects need to be taken into consideration, while evaluating MIMO channels in the presence of polarization diversity.

Channel Normalization

In order to isolate the small scale characteristics of the channel from the effects of shadowing and path-loss in the measured channel samples, we need to normalize the measured

channel matrix $\check{\mathbf{H}} = [\check{h}_{ij}]$ as $\mathbf{H} = \check{\mathbf{H}}/\mathcal{N}$. The channel capacity can then be calculated according to equation 3 for any reference SNR ρ. The normalization factor is generally defined as [31]

$$\mathcal{N} = \Big(\frac{1}{n_r n_t}\sum_i \sum_j E\{|\check{h}_{ij}|^2\}\Big)^{\frac{1}{2}} \tag{25}$$

This normalization would result in an average SISO SNR of unity on all the subchannels. This is appropriate for spatial MIMO channels for which $E\{||\mathbf{H}||_F^2\} = n_r n_t$. On the other hand, hybrid or dual-polarized configurations suffer from subchannel power losses, which need to be accounted for, in their capacity calculations. If the the normalization in (25) is used, the performance of these systems is overestimated. Thus in order to make a fair comparison with spatial configurations, we normalize the channel so as to achieve an average SISO SNR of unity on the elements of $\bar{\mathbf{H}}^{VV} = [\bar{h}_{ij}^{VV}]$. The normalization factor is calculated as

$$\bar{\mathcal{N}} = \left(\frac{1}{n_r^V n_t^V}\sum_i \sum_j E\big\{|\check{h}_{ij}^{VV}|^2\big\}\right)^{\frac{1}{2}} \tag{26}$$

Using the normalization in equation (26), leads to $E\{||\mathbf{H}^{VV}||_F^2\} = n_r^V n_t^V$ and the other subchannels scale accordingly to reflect the power losses. Thus this normalization provides a fair comparison between spatial and dual-polarized MIMO channels, for a constant transmit power.

4.3.1 Results for 2×2 MIMO

The 2×2 configuration is important for compact devices. The measurement data collected provided us with enough uncorrelated channel samples to evaluate cumulative capacity distribution functions (CDF), for 2×2 spatial and hybrid MIMO systems with an inter-element spacing $d \in \{\lambda/2, \lambda, 3\lambda/2, 2\lambda\}$. Capacity CDFs are calculated as per (3) at $\rho = 20$ dB. The array configurations considered are illustrated in Figure 17. The capacity CDFs obtained under LOS and NLOS channel conditions are plotted in Figures 18(a) and 18(b) respectively.

Under LOS channel conditions, it is evident that as the inter-element spacing d is made larger, the capacity of the spatial MIMO channel increases. This can be attributed to the decreasing subchannel correlation and to the spherical wavefront effects [26]. There is

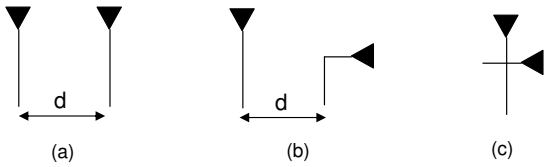

Figure 17: 2×2 Array configurations (a) Spatial (b) Hybrid (c) Dual-polarized

an increase of about 2.5 bps/Hz in median capacity for the spatial configuration as d is increased from $\lambda/2$ to 2λ. As d is increased, the capacity of hybrid MIMO channels also improves. But this could be attributed to only the spherical wavefront effects, because the subchannel correlations were found to be independent of d in our analysis in Section 4.2.3.

For $d = \lambda/2$, spatial and hybrid configurations achieve similar capacities. Furthermore, the dual-polarized configuration ($d = 0$), also performs equally well. We know from Section 4.2.3 that for small inter-element spacing, polarization based configurations achieve much lower subchannel correlation when compared to the spatial system. As a result they achieve higher capacity, despite the loss in subchannel powers. For higher values of d, even the spatial systems achieve lower subchannel correlation and as a result they outperform the hybrid systems, owing to the subchannel power losses incurred by the latter configuration.

Under NLOS channel conditions, it is evident from Table 3, that the correlation between the subchannels is low even for an inter-element spacing of $\lambda/2$. Hence the capacity does not significantly increase, as the spacing between the antenna elements is increased for the spatial configurations. Even the capacity of hybrid configurations is not very sensitive to variations in d.

From our measurements, the correlation values for dual-polarized/hybrid configurations are also very low in the NLOS channel. But these systems suffer from subchannel power losses because of high XPD and β values, which negatively effects the capacity. As a result, the spatial configurations outperforms the hybrid/dual-polarized configuration. For $d = \lambda/2$, the spatial configurations achieves an higher median capacity by about 1.5 bps/Hz over the co-located dual-polarized configuration.

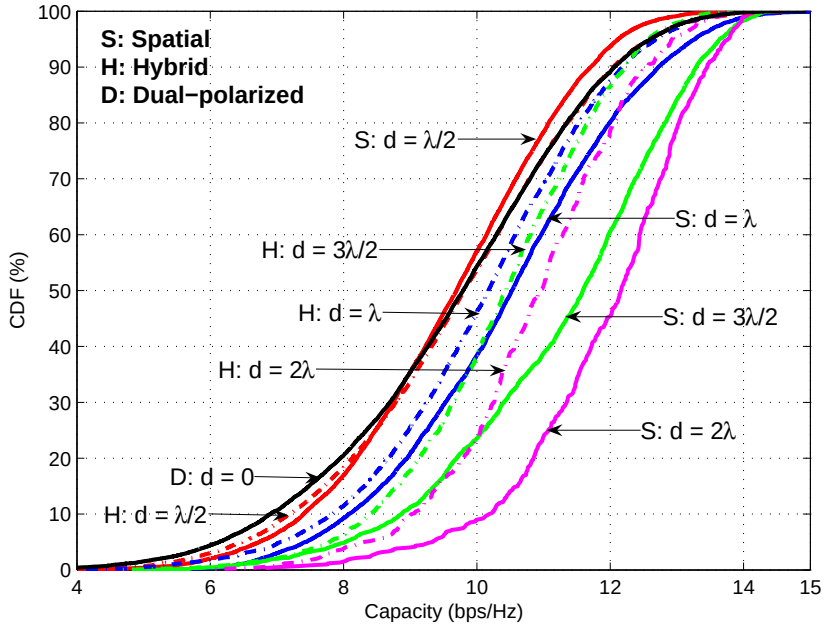

(a)

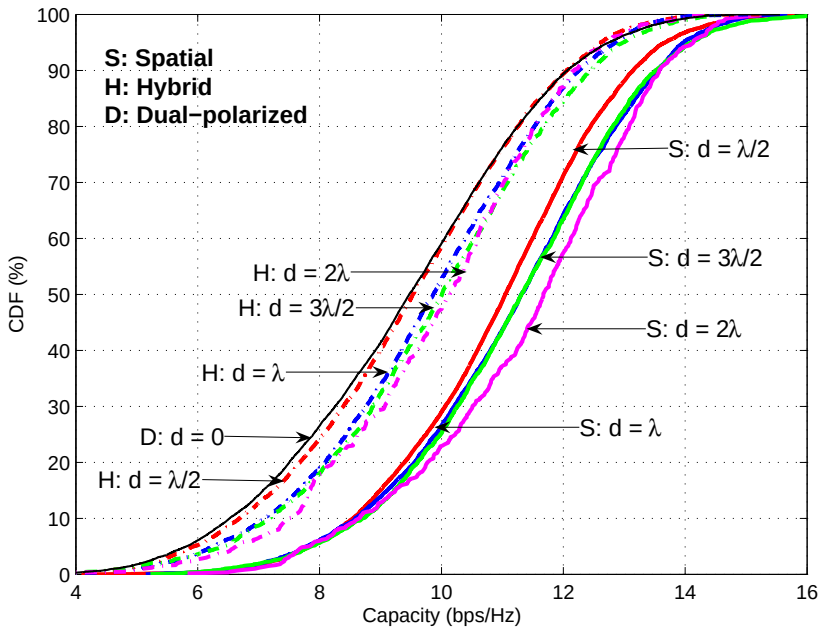

(b)

Figure 18: Capacity CDFs for 2×2 spatial, dual-polarized and hybrid MIMO channels at SNR $= 20$ dB under (a) LOS and (b) NLOS channel conditions

4.3.2 Results for 4×4 MIMO

4×4 configurations can be implemented in devices with larger form factors like notebook computers. With our measurement settings, we are limited to $d = \lambda/2$, when evaluating 4×4 spatial and hybrid MIMO channels. We consider dual-polarized configurations with $d \in \{\lambda/2, \lambda, 3\lambda/2, 2\lambda\}$. Note that a 4×4 dual-polarized configuration can be considered to be a special case of the hybrid configuration. Figures 20(a) and 20(b) depict the measured capacity CDFs under LOS and NLOS channel conditions respectively.

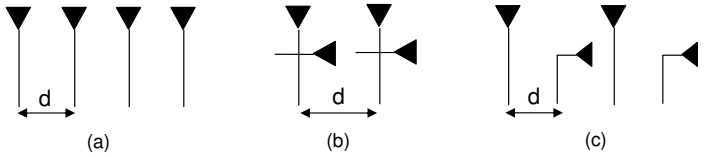

Figure 19: 4×4 Array configurations (a) Spatial (b) Dual-polarized (c) Hybrid

As expected, for all configurations, the 4×4 systems achieve higher capacity when compared to their corresponding 2×2 counterparts.

The spatial configuration performs better than the hybrid configuration owing to the loss in subchannel powers in the latter case. For the dual-polarized configuration, the performance improves by increasing the inter-element spacing. This is because of the decreasing correlation between the elements of the co-polar submatrices, $\mathbf{H}^{VV}$ and $\mathbf{H}^{HH}$. Further for $d = 3\lambda/2$, dual-polarized configuration performs slightly better than the spatial configuration with the same array length.

In the NLOS scenario, the capacity does not scale linearly with d. As for the 2×2 channels, the spatial system significantly outperforms both hybrid and dual-polarized configurations, once again owing to the subchannel power losses for the latter configurations. The spatial configuration with $d = \lambda/2$ performs about 1.5 bps/Hz better in median capacity, than the dual-polarized configuration of the same array length.

In addition to compactness, dual-polarized antennas could also be used to realize higher order MIMO architectures in compact devices. To underscore this point, we compare the capacity achieved by 2×2 spatial array configuration with $d = \lambda/2$ and the 4×4 dual-polarized MIMO configuration with the same array length. Under LOS channel conditions

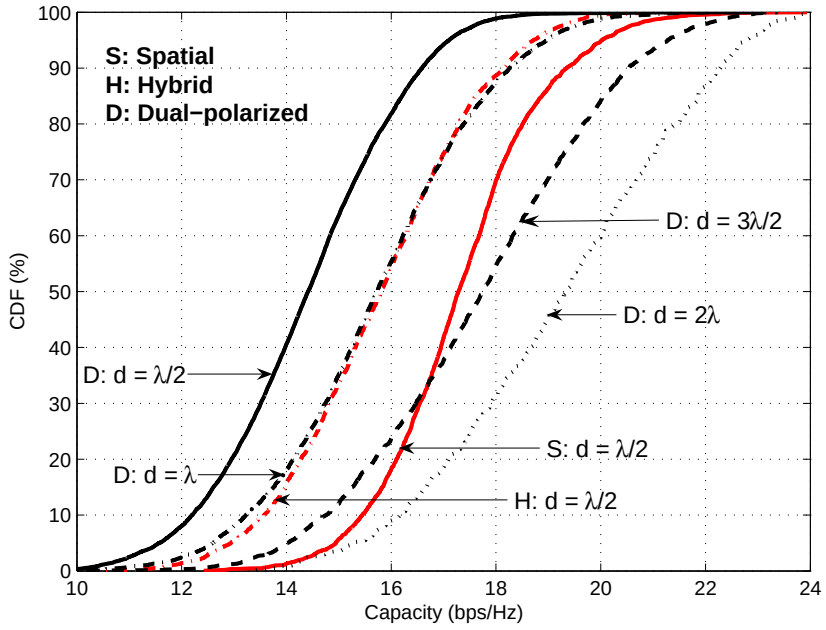

(a)

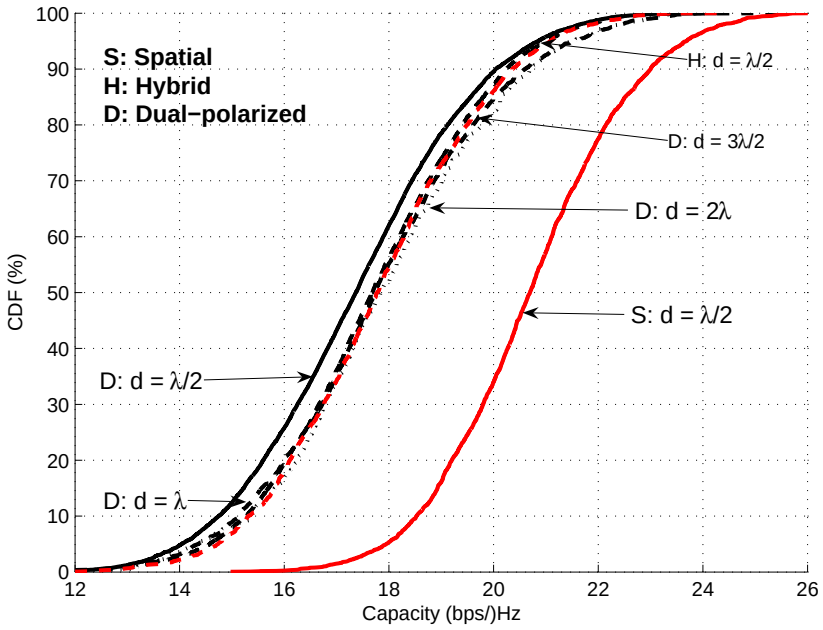

(b)

Figure 20: Capacity CDFs for 4×4 spatial, dual-polarized and hybrid MIMO channels at SNR $= 20$ dB under (a) LOS and (b) NLOS channel conditions

the 4×4 dual-polarized configuration achieves about 5 bps/Hz higher capacity than 2×2 spatial configuration. In the NLOS channel, this difference increases to 7 bps/Hz. Although the 4×4 configuration incurs no additional cost in terms of space, it requires 2 additional radio-frequency (RF) chains at the Tx and Rx, when compared to the spatial configuration.

These capacity results suggest than in systems wherein space is not a constraint, and large values of d are realizable, spatial systems should be preferred over hybrid or dual-polarized configurations, especially when the K-factor is low and the XPD is high. Our results provide no motivation for using the hybrid array configuration. However for devices like small sensors, wherein even a spatial array configuration with $d = \lambda/2$ cannot be realized, dual-polarized antennas offer an attractive alternative. Furthermore, dual-polarized antennas could be used to realize higher order architectures in devices with larger form factors, when compared to the spatial configuration.

CHAPTER V

ANTENNA SELECTION

In this thesis, we emphasize that the strategy of using only the "optimal" subset of all the available antennas, is all the more relevant for compact portable devices, which are often constrained by complexity, power and cost. Antenna selection, when combined with dual-polarized antennas, may be a solution that could enable compact systems to exploit the benefits of the MIMO architecture, with only a nominal increase in complexity. However, MIMO channels with polarization diversity cannot be modeled like pure spatial channels, because the subchannels of the MIMO channel matrix are not identically distributed [11]. They differ in terms of average received power, Ricean K-factor, cross-polar discrimination (XPD) and correlation properties, as discussed in the previous chapters. As a result, the performance of antenna selection for these channels needs to be evaluated. Antenna selection has been extensively studied in the context of spatial channels. However to the best of our knowledge, the issue of selection for dual-polarized MIMO channels has not been addressed in the literature.

In this chapter, we first study the impact of subchannel power losses on the selection gain achieved by $(2,1)/(2,1)$ selection for a dual-polarized Rayleigh MIMO channel. We analyze the performance of the popular capacity based selection approach, for dual-polarized MIMO configurations. We then consider systems employing VBLAST transmission. We evaluate the performance of MMSE based selection, in terms of BER, for these systems. Finally, we study antenna selection for dual-polarized MIMO systems employing OSTBC transmission. We provide a theoretical framework for analyzing the performance of norm-based selection for these systems. We use the measured channel samples collected in LOS and NLOS channel conditions, to compare the performance of antenna selection for spatial and dual-polarized MIMO configurations. In our analysis, we assume lossless RF switching. However, we caution that the insertion loss of RF switches degrades the performance of any

antenna selection system and should be taken into account, while designing these systems [44].

5.1 Effect of XPD on Selection Gain

The subchannels of a dual-polarized MIMO channels are not identically distributed. In this section we study the influence of subchannel power losses on gain achieved by using antenna selection. To make the analysis tractable, we consider a 2×2 dual-polarized MIMO channel. In this case the channel matrix (11) reduces to

$$\mathbf{H} = \begin{bmatrix} h^{VV} & h^{VH} \\ h^{HV} & h^{HH} \end{bmatrix}. \tag{27}$$

All the subchannels are assumed to be independent circularly symmetric complex Gaussian random variables. This is an appropriate assumption for the typical NLOS indoor channel as seen in the previous chapter. Further, we make the simplifying assumptions that $X_V = X_H = X$, $1 \leq X < \infty$ and $\beta = 1$. We note that when $X = 1$, dual-polarized MIMO channel is equivalent to a spatial channel.

For (2,1)/(2,1) selection, the optimal strategy would be to select the subchannel which has the maximum instantaneous power. The instantaneous post processing SNR for the selected SISO channel ($\tilde{h}$) is given by YE_s/N_o, where the random variable, $Y = |\tilde{h}|^2$. If h is a CSCG random variable with zero mean and variance σ^2, the cumulative distribution function (CDF) of $Z = |h|^2$ is given by, $F_Z(z) = (1 - e^{-z/\sigma^2})U(z)$, where $U(z)$ is the unit step function. Since all the elements of $\mathbf{H}$ are assumed to be mutually independent, the CDF of Y can be derived as follows

$$\begin{aligned} F_Y(y) &= Pr(|h^{VV}|^2 < y)Pr(|h^{HH}|^2 < y)Pr(|h^{HV}|^2 < y)Pr(|h^{VH}|^2 < y) \\ &= Pr(|h^{VV}|^2 < y)^2 Pr(|h^{HV}|^2 < y)^2 \\ &= (1 - e^{-y})^2(1 - e^{-yX})^2 U(y). \end{aligned} \tag{28}$$

The probability density function (PDF), $f_Y(y) = \frac{dF_Y(y)}{dy}$ is given by

$$\begin{aligned} f_Y(y) &= 2\Big(e^{-y}(1-e^{-y})(1-e^{-yX})^2 + Xe^{-yX}(1-e^{-yX})(1-e^{-y})^2\Big)U(y) \\ &= 2\Big(e^{-y}(1-e^{-y}) + Xe^{-yX}(1-e^{-yX}) + (1+2X)e^{-y(1+2X)} \\ &\quad +(2+X)e^{-y(2+X)} - (1+X)e^{-y(1+X)}(2+e^{-y(1+X)})\Big)U(y). \end{aligned} \tag{29}$$

Using the identity, $\int_0^\infty x^n e^{-ax}dx = n!/a^{n+1}$, the n-th moment of Y can be computed to be

$$\begin{aligned} E\{Y^n\} &= 2n!\Bigg[\left(1+\frac{1}{X^n}\right)\left(1-\frac{1}{2^{n+1}}\right) + \frac{1}{(1+2X)^n} + \frac{1}{(2+X)^n} \\ &\quad -\frac{2}{(1+X)^n}\left(1+\frac{1}{2^{n+2}}\right)\Bigg]. \end{aligned} \tag{30}$$

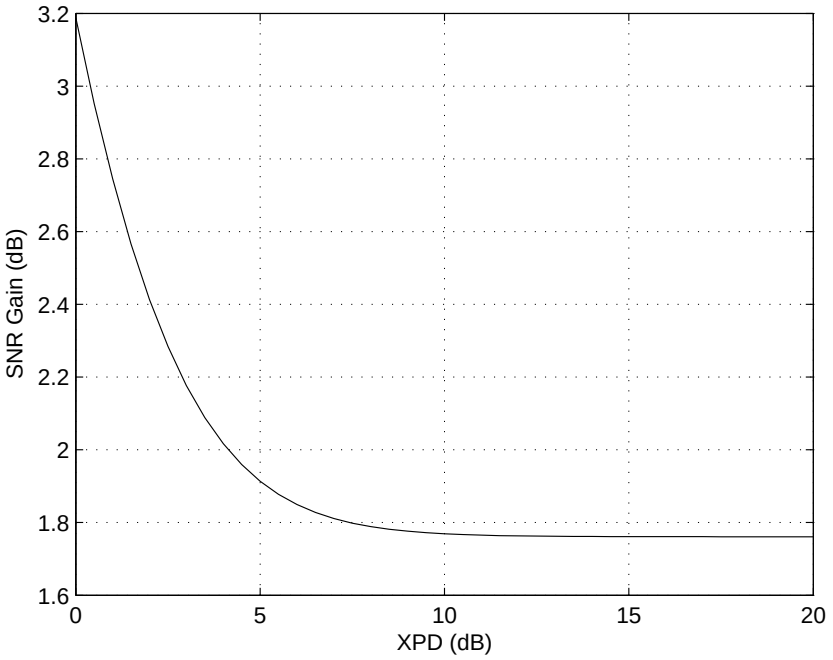

Figure 21: Effect of XPD on (2,1)/(2,1) selection gain

The gain in average SNR, achieved by using antenna selection is $G(X) = E\{Y\}$, and can be evaluated from (30) to be

$$G(X) = \frac{3(1+X)}{2X} + \frac{2}{1+2X} + \frac{2}{2+X} - \frac{9}{2(1+X)} \tag{31}$$

The average SNR gain is a monotonically decreasing function of X, as shown in Figure 21. The selection gain is maximum at 3.2 dB when $X = 1$ and asymptotically diminishes to 1.76 dB as $X \to \infty$. These values are consistent with the well known result for SNR gain of selection diversity with M independent and equal powered Rayleigh diversity branches, given by $\sum_{i=1}^{M} \frac{1}{i}$ [5].

The probability that one of the cross-polar subchannels is selected can be computed as follows

$$\begin{aligned} P(X) &= Pr\{(\tilde{h} = h^{VH}) \cup (\tilde{h} = h^{HV})\} \\ &= 2 \cdot Pr\{h^{VH} > h^{HV}\} \cdot Pr\{h^{VH} > h^{HH}\} \cdot Pr\{h^{VH} > h^{VV}\} \\ &= 2 \cdot (1/2) \cdot Pr\{h^{VH} > h^{HH}\}^2 \\ &= \frac{1}{(1+X)^2} \end{aligned} \tag{32}$$

As the XPD increases, the probability of the cross-polar subchannels being selected decreases and thus the average SNR gain diminishes. Further, $\lim_{X\to\infty} P(X) = 0$, which indicates that in the limiting case, the available degrees of diversity reduce to 2, when compared to 4 for $X = 1$. Thus a high XPD results in a diversity loss for dual-polarized MIMO channels, when compared to spatial channels.

Shown in Figure 22, is the standard deviation of the instantaneous SNR gain, Y. It is calculated as $\sigma_Y(X) = \sqrt{E\{Y^2\} - E\{Y\}^2}$. It is interesting to note that $\sigma_Y(X)$ is not a monotonic function of X. It takes a maximum value of 0.75 dB for $X = 1$, a minimum value of 0.24 dB for $X = 2.5$ and approaches 0.48 dB as $X \to \infty$.

Similar analysis can be done for the parameter β. As a result of these subchannel power losses, antenna selection for dual-polarized MIMO channels performs under par when compared to uncorrelated spatial channels. However, it is well known that correlation between the diversity branches reduces the selection gain. Thus in environments where the spatial channel is highly correlated, this performance gap diminishes.

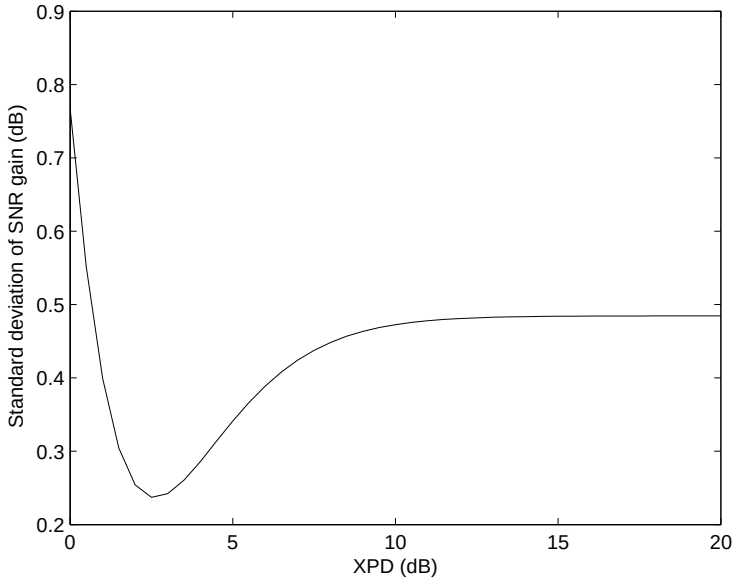

Figure 22: Standard deviation of the SNR gain achieved by $(2,1)/(2,1)$ selection

5.2 Capacity-based Selection

A popular approach to antenna selection for spatial MIMO channels has been to select the best subset of transmit and receive antennas to maximize the mutual information. First proposed in [18], this strategy has been extensively studied in the literature (See [37] and the references therein). It has been shown that capacity based antenna selection achieves the diversity order of a full system, for spatial channels [37]. In this section, we study the performance of this approach for dual-polarized MIMO channels.

For a given $l_r \times l_t$ MIMO channel matrix, $\bar{\mathbf{H}}$, according to equation (3), channel capacity at a reference SNR of ρ can be evaluated as $C(\bar{\mathbf{H}}) = \log_2(\det(\mathbf{I}_{l_r} + \frac{\rho}{l_t}\bar{\mathbf{H}}\bar{\mathbf{H}}^H))$. The strategy for $(n_r, l_r)/(n_t, l_t)$ selection can then be expressed as [18]:

$$\widetilde{\mathbf{H}} = arg \min_{S(\bar{\mathbf{H}})} \{C(\bar{\mathbf{H}})\}, \tag{33}$$

where $\bar{\mathbf{H}}$ is obtained by eliminating $n_r - l_r$ columns and $n_t - l_t$ rows from $\mathbf{H}$. $S(\bar{\mathbf{H}})$ denotes the set of all possible $\bar{\mathbf{H}}$, whose cardinality is $\binom{n_r}{l_r}\binom{n_t}{l_t}$. In this thesis, we assume optimal selection, but we note that efficient algorithms for implementing this strategy can be found in [16, 21, 41].

To study the effect of XPD on the capacity of dual-polarized MIMO systems with antenna selection, we consider a $(2,1)/(2,1)$ system under similar assumptions as in Section 5.1. In this case, the ergodic capacity of the optimally selected SISO link is given by

$$E\{C\} = \int_{-\infty}^{\infty} \log_2(1+\rho(y)) f_Y(y) dy \tag{34}$$

where $\rho(y) = yE_s/N_o$ is the instantaneous output SNR of the selected SISO link and $f_Y(y)$ has been evaluated in (29). Shown in Figure 23, is the numerically evaluated ergodic capacity curves for different values of the XPD. Also shown in there is ergodic capacity curve for deterministic (or "no") selection case. It is evident that the ergodic capacity

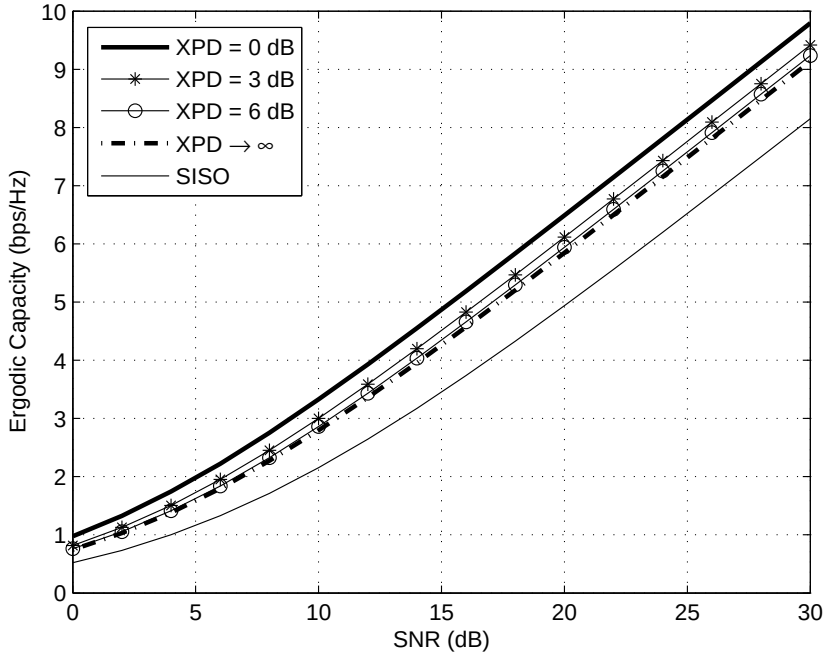

Figure 23: Effect of XPD on the capacity of (2,1)/(2,1) dual-polarized MIMO channels

is maximum for $X = 1$ and approaches the limiting case ($X \to \infty$) curve as the XPD increases. However, we argue that inspite of the degradation in capacity for high XPD, antenna selection with dual-polarized antennas performs much better than deterministic selection. For example at SNR = 20 dB, selection with dual-polarized antennas provides a minimum gain of 0.9 bps/Hz, while selection with spatial MIMO offers a gain of 1.5 bps/Hz. Note that, unlike the spatial configuration, the dual-polarized configuration does not incur

any additional cost in terms of space, when compared to the SISO system.

5.2.1 Measurement Results

In this section we analyze the performance of antenna selection in terms of ergodic capacity for dual-polarized and spatial MIMO systems, using the measured channel samples. We consider (2,1)/(2,1) and (4,2)/(4,2) optimal antenna selection according to the criteria outlined in (33), under LOS and NLOS channel conditions, for a range of values of inter-element spacing. We use exhaustive search to achieve optimal selection.

In Figures 24(a) and 24(b), we plot the capacity curves for (2,1)/(2,1) selection under LOS and NLOS channel conditions, respectively. We consider a 2×2 dual-polarized (D) system with $L = 0$ and a spatial (S) system with $L = \lambda/2$. For reference, we also plot the BER for a vertically polarized deterministic SISO link. In all the following figures, DS stands for deterministic selection.

In the results for the hallway, shown in Figure 24(a), the dual-polarized system with selection outperforms the SISO link by about 0.7 bps/Hz at SNR = 20 dB. The spatial system with selection performs better than its dual-polarized counterpart by about 0.3 bps/Hz, owing to the subchannel power losses in the latter configuration. This difference is not larger, because the spatial MIMO with $L = \lambda/2$ suffers from high subchannel correlations as discussed in Section 4.2.3.

Under NLOS channel conditions, the dual-polarized system with selection outperforms the SISO link by 0.5 bps/Hz at SNR = 20 dB. The performance gap between the spatial and dual-polarized systems, in the presence of selection, increases to 0.6 bps/Hz. This is because in the NLOS scenario, the spatial MIMO channel achieves significant decorrelation and hence achieves full diversity. On the other hand, dual-polarized configuration suffers from subchannel power losses.

In addition to providing compactness, dual-polarized antennas can also be used to realize higher order MIMO configurations in devices with larger form factors. In Figures 25(a) and 25(b), we plot the capacity curves for (4,2)/(4,2) selection under LOS and NLOS channel conditions respectively. A four element dual-polarized array can be realized as shown in

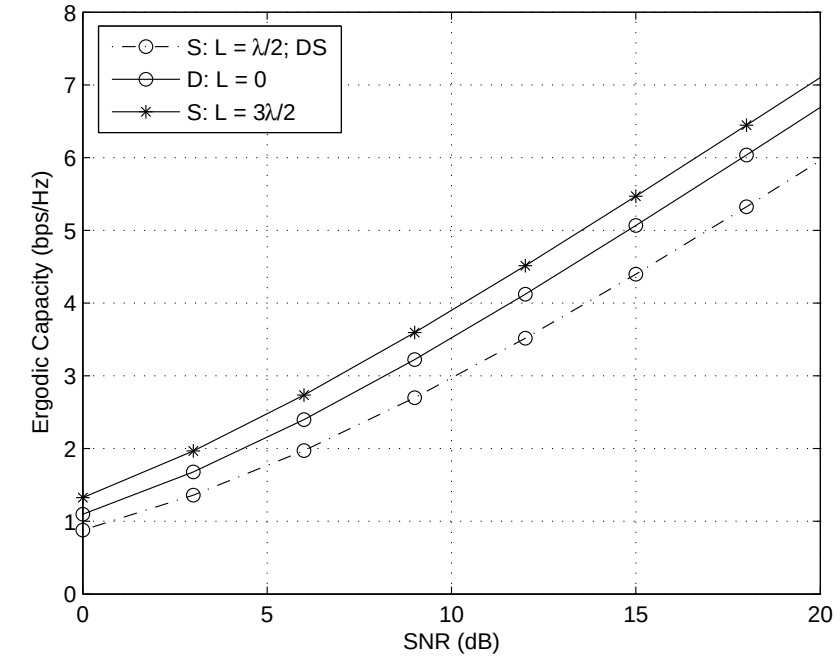

(a)

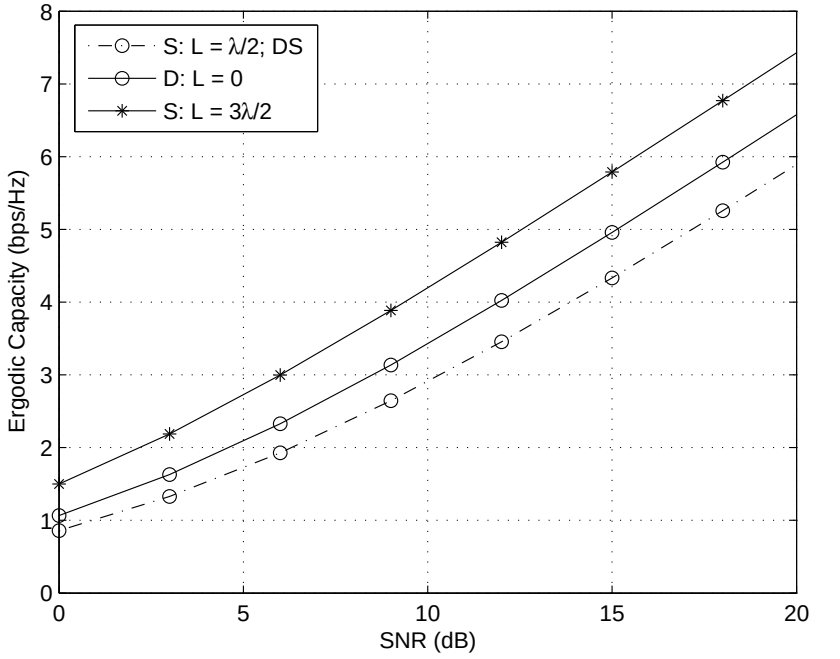

(b)

Figure 24: Measured capacities of (2,1)/(2,1) antenna selection under (a) LOS and (b) NLOS channel conditions

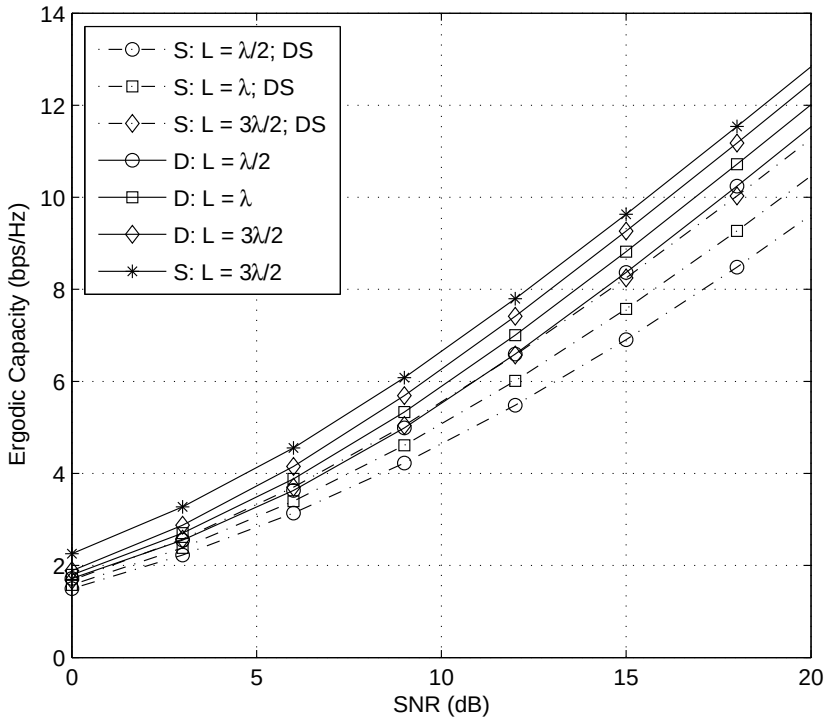

(a)

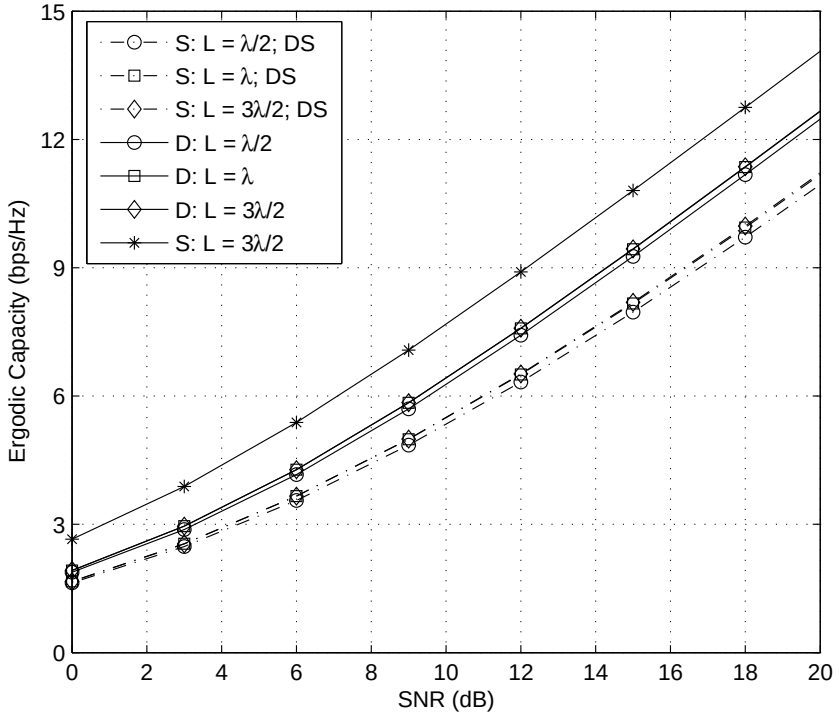

(b)

Figure 25: Measured capacities of (4,2)/(4,2) antenna selection under (a) LOS and (b) NLOS channel conditions

Figure 19. This configuration could be useful for the not-so-compact handheld devices like notebook computers. In these figures, we consider a 4×4 dual-polarized system with $L \in \{\lambda/2, \lambda, 3\lambda/2\}$ and a spatial system with $L = 3\lambda/2$. The minimum inter-element spacing between the adjacent antenna elements is maintained at $\lambda/2$. For reference we also plot the BER for deterministic selection (DS) for 2×2 spatial MIMO with $L \in \{\lambda/2, \lambda, 3\lambda/2\}$.

In the hallway, as the inter-element spacing is increased, the performance of the 2×2 spatial MIMO with deterministic selection improves owing to the decrease in the subchannel correlations and the spherical wavefront effect [26]. Further the performance of the 4×4 dual-polarized MIMO with selection also improves with increasing inter-element spacing because of the lower correlations between the elements of the co-polar submatrices $\mathbf{H}^{VV}$ and $\mathbf{H}^{HH}$. It is interesting to observe that the $(4,2)/(4,2)$ dual-polarized configuration, with $L = \lambda/2$, performs as well as the 2×2 deterministic spatial MIMO with $L = 3\lambda/2$, thus providing compactness.

Under NLOS channel conditions, as expected, the performance is not a strong function of the inter-element spacing. For $L = \lambda/2$, the 4×4 dual-polarized system with selection outperforms the 2×2 deterministic spatial MIMO by 1.5 bps/Hz at SNR = 20 dB. The (4,2)/(4,2) spatial MIMO with $L = 3\lambda/2$ outperforms the dual-polarized MIMO with selection by about 1.5 bps/Hz.

These results suggest that antenna selection with dual-polarized antennas could achieve higher capacities than spatial systems without selection. More importantly, these configurations do not incur any additional expense in terms of space.

5.3 Selection for Layered Space-Time Systems with Linear Receivers

The capacity based approach discussed in the previous section has been very popular. However, such antenna selection solutions are unlikely to achieve optimum error performance for systems with limited complexity receivers [6, 14]. Hence selection criteria have to be tailored to different receiver implementations. In this section we consider VBLAST transmission with linear minimum mean squared error (MMSE) receiver signal processing [5].

Different approaches to minimize the error rates of spatial multiplexing systems using linear receivers have been proposed in the literature [14, 19, 6]. In this thesis, we consider the MMSE based antenna selection approach proposed in [14], which has been shown to out-perform other techniques for spatial multiplexing systems with linear MMSE receivers. We note that a similar approach can be used for systems with zero-forcing (ZF) receivers.

Consider a $l_r \times l_t$ MIMO channel given by $\bar{\mathbf{H}}$. The basic premise of the VBLAST transmission technique is to leverage the multiplexing gain provided by the MIMO architecture, to achieve higher data rates. The number of parallel symbol streams that can be simultaneously transmitted is limited by the rank of the channel matrix. The data stream is multiplexed into l_t parallel streams which are then independently encoded and transmitted using the l_t antennas [12]. The input-output relation for this system can be expressed as

$$\mathbf{r} = \sqrt{\frac{E_s}{l_t}}\bar{\mathbf{H}}\mathbf{s} + \mathbf{n},$$

where $\mathbf{r} = [r_i], 1 \leq i \leq l_r$ and $\mathbf{s} = [s_j], 1 \leq j \leq l_t$ are the baseband complex received and transmitted signal vectors respectively. It is assumed that the data streams on each antenna are uncorrelated and hence $E\{\mathbf{s}\mathbf{s}^H\} = \mathbf{I}_{l_t}$. $\mathbf{n}$ represents the complex circular Gaussian noise vector with covariance matrix $R_{nn} = N_o\mathbf{I}_{\mathbf{l_r}}$. E_s denotes the total transmit signal power. We define SNR as E_s/N_o.

The task of the receiver is to jointly detect the transmitted symbol vector $\mathbf{s}$, by suppressing the interference presented by one stream on the other. Both linear and non-linear receiver structures can be implemented. Linear interference suppression techniques like linear MMSE and ZF are easy to implement and perform significantly better than the matched filter receiver. Non-linear techniques such as successive interference cancellation (SIC) and parallel interference cancellation (PIC), outperform the linear techniques, but incur significant processing complexity. As the motivation for this work is to explore low-complexity MIMO techniques for compact portable devices, we consider only linear MMSE receiver signal processing.

5.3.1 MMSE-based Selection

If the receiver employs a linear MMSE (LMMSE) detector, it uses a spatial filter $\mathbf{w}$ on the received signal vector $\mathbf{r}$, so as to minimize the mean squared error given by [5]

$$\begin{aligned} \text{MSE} &= E\{||\mathbf{w}^H\mathbf{r}-\mathbf{s}||^2\} \\ &= \text{tr}\left[E\left\{\left(\mathbf{w}^H\mathbf{r}-\mathbf{s}\right)\left(\mathbf{w}^H\mathbf{r}-\mathbf{s}\right)^H\right\}\right] \\ &= \text{tr}\left[\left(\mathbf{w}^H-\bar{\mathbf{H}}^H\mathbf{R}_r^{-1}\right)\mathbf{R}_r\left(\mathbf{w}^H-\bar{\mathbf{H}}^H\mathbf{R}_r^{-1}\right)^H+\left(\mathbf{I}_{l_r}-\bar{\mathbf{H}}^H\mathbf{R}_r^{-1}\bar{\mathbf{H}}\right)\right], \end{aligned} \tag{35}$$

where, $\mathbf{R_r}=\bar{\mathbf{H}}\bar{\mathbf{H}}^H+N_o\mathbf{I}_{l_r}$ and $\text{tr}(\mathbf{A})$ denotes the trace of the matrix $\mathbf{A}$. Since only the first term in equation (35) depends on $\mathbf{w}$, the MMSE solution chooses $\mathbf{w}_{\text{opt}}=\mathbf{R_r}^{-1}\bar{\mathbf{H}}$, so as to make it zero. Now the residual minimum mean squared error, is given by

$$\xi(\bar{\mathbf{H}})=\text{tr}(\mathbf{I}_{l_r}-\bar{\mathbf{H}}^H\mathbf{R}_r^{-1}\bar{\mathbf{H}}). \tag{36}$$

The MMSE based antenna selection approach is devised to minimize this residual error [14]. As is evident from equation (36), the residual error is a function of $\bar{\mathbf{H}}$. For $(n_r,l_r)/(n_t,l_t)$ antenna selection, the selection criteria can be expressed as follows [14]:

$$\widetilde{\mathbf{H}}=arg\min_{S(\bar{\mathbf{H}})}\{\xi(\bar{\mathbf{H}})\}, \tag{37}$$

where $\bar{\mathbf{H}}$ is obtained by eliminating n_r-l_r columns and n_t-l_t rows from $\mathbf{H}$. $S(\bar{\mathbf{H}})$ denotes the set of all possible $\bar{\mathbf{H}}$, whose cardinality is $\binom{n_r}{l_r}\binom{n_t}{l_t}$. In this paper we assume optimal selection, but we note that practical suboptimal algorithms to implement this strategy have been proposed and they achieve near-optimal performance [14].

In order to study the influence of XPD on the bit-error-rate (BER) of dual-polarized MIMO systems with antenna selection, we consider a $(2,1)/(2,1)$ system under similar assumptions as in Section 5.1. We note that the strategy outlined in (37) reduces to selecting the subchannel which has the maximum instantaneous power. So the analysis performed in Section 5.1 is applicable here.

For a given channel $\mathbf{H}$, the bit error rate (BER) with Gray mapped 4-QAM constellation, $Pr(\text{error}/\mathbf{H})=Q(\sqrt{\frac{2Y E_b}{N_o}})$ where $E_b/N_o=E_s/(2l_tN_o)$ is the pre-detection SNR per bit and

$Q(x) = \frac{1}{\sqrt{2\pi}} \int_x^\infty e^{-\frac{t^2}{2}} dt$. The average BER can be calculated as:

$$\text{BER} = \int_{-\infty}^{\infty} Q\left(\sqrt{\frac{yE_s}{N_o}}\right) f_Y(y) dy \tag{38}$$

For a spatial MIMO channel, a closed form expression for BER can be developed and it can

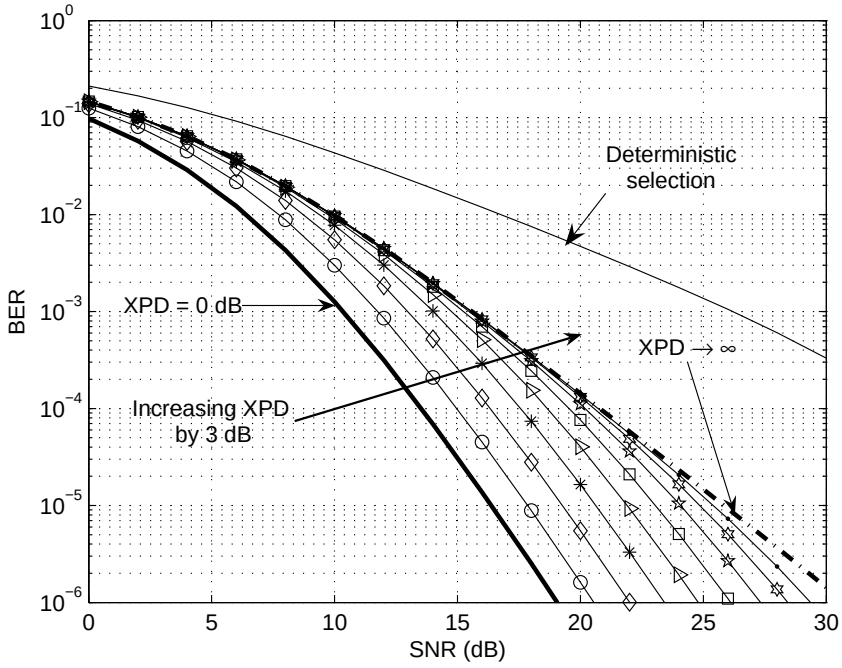

Figure 26: Numerically evaluated BER curves for (2,1)/(2,1) selection for different XPD

be shown that at high SNR, BER $\propto \frac{1}{(E_s/N_o)^\eta}$ [5]. As mentioned previously, the two extreme cases i.e. $X = 1$ and $X \to \infty$ result in diversity orders $\eta = 4$ and $\eta = 2$, respectively. However, for other values of X it is not easy to arrive at such insightful approximations. Hence to analyze the influence of XPD on BER, we numerically evaluate (38). As shown in Figure 26, as the XPD increases, BER performance of selection diversity deteriorates.

The measured NLOS XPD values reported in the literature, for indoor environments vary between 0 to 9 dB [31, 51]. From Figure 26, we observe that the BER curve corresponding to $X = 9$ dB, is extremely close to the worst-case ($X \to \infty$) curve for SNR < 8 dB. However as the SNR increases, $X = 9$ dB yields a BER that is significantly better than the worst-case.

Similar analysis can be done for the parameter β. As a result of these subchannel

power losses, antenna selection for dual-polarized MIMO channels performs under par when compared to spatial channels. However in environments where the spatial channel is highly correlated, the performance gap diminishes as shown in our measurement results.

5.3.2 Measured Channel Results

In this section we analyze the performance of antenna selection in terms BER, for dual-polarized MIMO systems employing VBLAST transmission and linear MMSE receiver signal processing. The measured channel samples are used to achieve this objective. The measured MIMO channel samples were normalized to achieve $E\{||\mathbf{H}^{VV}||_F^2\} = n_r^V n_t^V$ as discussed in Section 4.3.

The input symbols s_i were drawn from an equiprobable 4-QAM constellation $\{\pm 1 \pm j\}/\sqrt{2}$. The channel was assumed to be static for a frame of 100 symbols. BER is calculated for each frame and averaged over the N channel realizations provided by the measurements (See Table 4.1). The array length is the same at the transmitter and the receiver. We consider (2,1)/(2,1) and (4,2)/(4,2) optimal antenna selection according to the criteria outlined in (37), under LOS and NLOS channel conditions, for a range of values of inter-element spacing. We use exhaustive search to achieve optimal selection.

In Figures 27(a) and 27(b), we plot the BER curves for (2,1)/(2,1) selection under LOS and NLOS channel conditions, respectively. We consider a 2×2 dual-polarized (D) system with $L = 0$ and a spatial (S) system with $L = \lambda/2$. For reference we also plot the BER for a vertically polarized deterministic SISO link. In all the following figures, DS stands for deterministic (or "no") selection.

In the results for the hallway, shown in Figure 27(a), the dual-polarized system with selection outperforms the SISO link by 8 dB at BER = 10^{-2}. The spatial system with selection performs better than its dual-polarized counterpart by about 1 dB, owing to the subchannel power losses in the latter configuration. This difference is not larger because the spatial MIMO with $L = \lambda/2$ suffers from high subchannel correlations (Table 3).

Under NLOS channel conditions, the dual-polarized system with selection outperforms

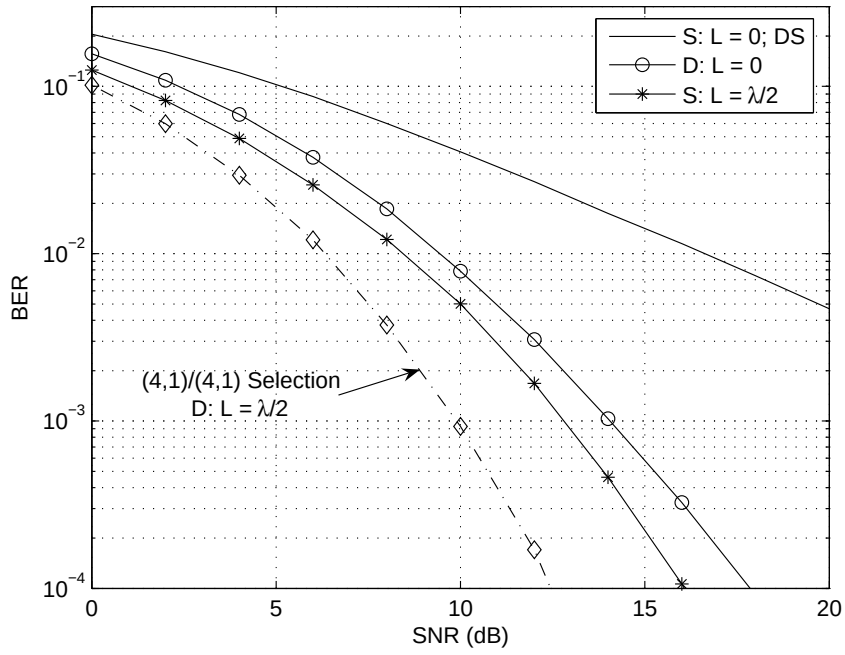

(a)

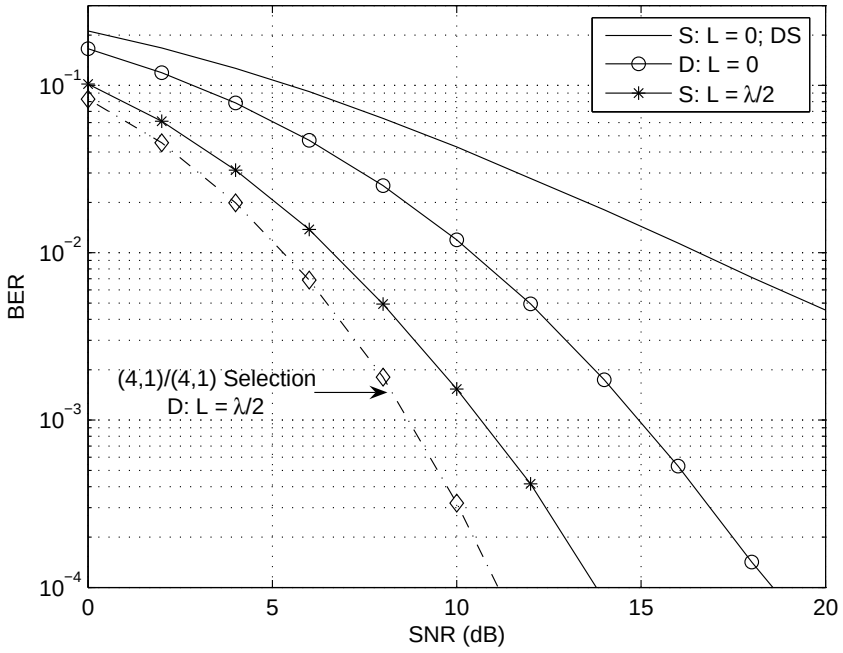

(b)

Figure 27: BER over measured channels for (2,1)/(2,1) antenna selection for a VBLAST system with LMMSE receiver under (a) LOS and (b) NLOS channel conditions

the SISO link by 6 dB at BER $= 10^{-2}$. The performance gap between the spatial and dual-polarized systems, in the presence of selection, increases to 3.5 dB. This is because in NLOS scenarios, a spatial MIMO channel achieves significant decorrelation and hence achieves full diversity. On the other hand, dual-polarized configuration suffers from subchannel power losses. We emphasize that despite these losses, dual-polarized antennas offer the distinct benefit of compactness over the spatial configuration.

In addition to providing compactness, dual-polarized antennas can also be used to realize higher order MIMO configurations in devices with larger form factors. To underscore this point, we also plot in Figures 27(a) and 27(b), BER results for (4,1)/(4,1) selection with dual-polarized antennas. This configuration could be realized in the same space as the (2,1)/(2,1) spatial configuration, yet it achieves better performance under both LOS and NLOS channel conditions.

In Figures 28(a) and 28(b), we plot the BER curves for (4,2)/(4,2) selection under LOS and NLOS channel conditions respectively. In these figures, we consider a 4×4 dual-polarized system with $L \in \{\lambda/2, \lambda, 3\lambda/2\}$ and a spatial system with $L = 3\lambda/2$. The minimum inter-element spacing between the adjacent antenna elements is maintained at $\lambda/2$. For reference we also plot the BER for deterministic selection (DS) for 2×2 spatial MIMO with $L \in \{\lambda/2, \lambda, 3\lambda/2\}$.

In the hallway, as the inter-element spacing is increased, the performance of the 2×2 spatial MIMO with deterministic selection improves, owing to the decrease in the subchannel correlations and the spherical wavefront effect [26]. Further the performance of the 4×4 dual-polarized MIMO with selection also improves with increasing inter-element spacing because of the lower correlations between the elements of the co-polar submatrices $\mathbf{H}^{VV}$ and $\mathbf{H}^{HH}$. For an array length of $L = 3\lambda/2$, the 4×4 spatial and dual-polarized MIMO systems perform equally well. They achieve a selection gain of 8 dB at BER $= 10^{-2}$.

Under NLOS channel conditions, as expected, the performance is not a strong function of the inter-element spacing. For $L = \lambda/2$, the 4×4 dual-polarized system with selection outperforms the 2×2 deterministic spatial MIMO by 8.5 dB at BER $= 10^{-2}$. The (4,2)/(4,2) spatial MIMO with $L = 3\lambda/2$ outperforms the dual-polarized MIMO with selection by about

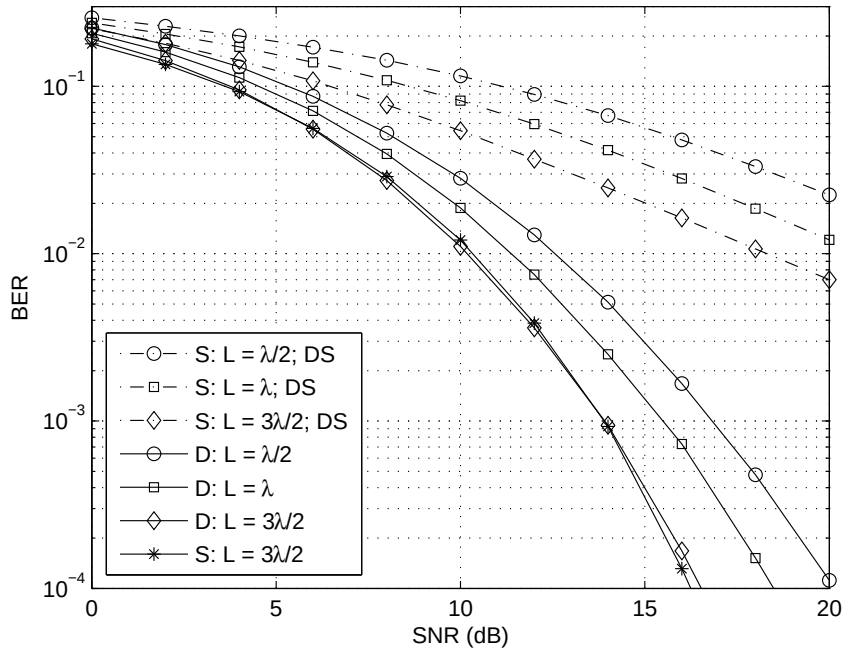

(a)

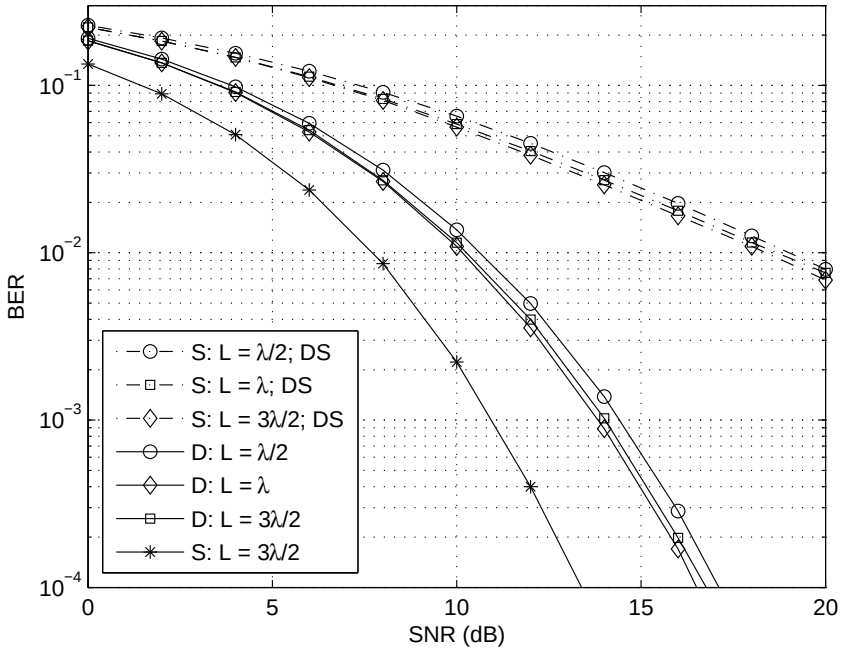

(b)

Figure 28: BER over measured channels for (4,2)/(4,2) antenna selection for a VBLAST system with LMMSE receiver under (a) LOS and (b) NLOS channel conditions

2.5 dB.

These measurement results indicate that while antenna selection with the spatial array configuration performs the best under both LOS and NLOS channel conditions, it requires a larger array length which is not always possible to realize in compact devices. On the other hand, antenna selection with dual-polarized antennas performs significantly better than deterministic selection, with only a nominal increase in complexity and with no cost in terms of space.

5.4 Selection for Space Time Coded Systems

Unlike the layered BLAST architectures which attempt to increase the transmitted data rate, space-time coding is a technique which increases the reliability of data transmission by exploiting the diversity of a MIMO channel. Orthogonal space time block coding (OSTBC), has received much interest owing to its simple linear decoding process. Antenna selection for spatial MIMO channels with OSTBC has been studied in [20]. In this section, we follow the same approach as [20], to study the performance of antenna selection for dual-polarized MIMO systems with OSTBC transmission.

We first briefly review the popular Alamouti space time block coding scheme, which is an example of OSTBC with two transmit antennas. The Alamouti space time block code is a simple and an effective way to exploit the diversity of a MIMO channel. It does not require channel knowledge at the transmitter, but yet it achieves full diversity order. Consider a $n_r \times 2$ MIMO channel matrix $\mathbf{H} = [\mathbf{h}_1, \mathbf{h}_2]$. To send a pair of symbols $\mathbf{s} = [s_1, s_2]^T$, a transmitter with two antennas that uses the Alamouti STBC requires two signaling intervals. Here $\mathbf{A}^T$ is the transpose of the matrix $\mathbf{A}$. The code matrix can be written as [2]

$$\mathbf{C}(\mathbf{s}) = \begin{bmatrix} s_1 & -s_2^* \\ s_2 & s_1^* \end{bmatrix}. \tag{39}$$

The rows of the code matrix denote the spatial dimension and the columns, the temporal dimension. If $\mathbf{r}_i, i \in \{1, 2\}$ denotes the received signal vector in the i-th signaling interval.

The input-output relationship for the system can be written as [5]

$$\mathbf{r} = \sqrt{\frac{E_s}{n_t}}\mathbf{H}_{\text{eff}}\mathbf{s} + \mathbf{n}, \tag{40}$$

where $n_t = 2$, $\mathbf{r} = [\mathbf{r}_1^T, \mathbf{r}_2^T]^T$ and $\mathbf{n}$ represents the circularly symmetric complex Gaussian noise vector with covariance matrix $R_{nn} = N_o\mathbf{I_{2n_r}}$. The effective $2n_r \times 2$ MIMO channel matrix is given by

$$\mathbf{H}_{\text{eff}} = \begin{bmatrix} \mathbf{h}_1 & \mathbf{h}_2 \\ \mathbf{h}_2^* & -\mathbf{h}_1^* \end{bmatrix}. \tag{41}$$

The joint maximum likelihood (JML) receiver chooses $\hat{\mathbf{s}} = [\hat{s_1}, \hat{s_2}]^T$ to minimize $E\{||\mathbf{r} - \mathbf{H}_{\text{eff}}\hat{\mathbf{s}}||^2\}$. Note that the matrix $\mathbf{H}_{\text{eff}}$ is orthogonal i.e. $\mathbf{H}_{\text{eff}}^H\mathbf{H}_{\text{eff}} = \|\mathbf{H}\|_F^2\mathbf{I}_2$. As a result, the JML receiver reduces to a simple matched filter receiver. The effective instantaneous post-detection SNR for the data stream is

$$\gamma = \frac{E_s}{n_t N_o}\|\mathbf{H}\|_F^2. \tag{42}$$

Note that the Alamouti code is a full-rate linear orthogonal code for $n_t = 2$ [5]. Further it achieves maximal diversity, and owing to the simple receiver implementation, it is an attractive transmission scheme for low-complexity systems. General orthogonal space time codes for $n_t > 2$ transmit antennas can be designed using the *rank* and *determinant* criterion outlined in [47]. Even in this case, equation (42) is valid. However it has been shown that there exists no full-rate OSTBC for $n_t > 2$ [47]. Inspite of the loss in rate, the higher order OSTBC could still be used, owing to the simple receiver implementation.

5.4.1 Performance of OSTBC in the presence of Polarization Diversity

In this section, we digress from the topic of antenna selection to study the performance of OSTBC in dual-polarized MIMO channels. The squared Frobenius norm of the channel, $W = \|\mathbf{H}\|_F^2$, defined in equation (2), is a random variable. For a $n_r \times n_t$ i.i.d Rayleigh spatial MIMO channel, W is a chi-squared random variable with $\eta = n_r n_t$ degrees of freedom, with PDF given by

$$f_W(w) = \frac{w^{\eta-1}e^{-w}}{(\eta-1)!} \tag{43}$$

However for a dual-polarized MIMO channel, the subchannels are non-identical and hence the above equation is not valid. We assume that $\beta = 1$ and $X_V = X_H = X$. The PDF can then be derived to be

$$f_W(w) = \frac{X^{n_x} e^{-w} w^{(n_c-1)}}{(n_x-1)!(n_c-1)!} \sum_{k=0}^{n_c-1} \binom{n_c-1}{k} \frac{(-1)^k (n_x+k-1)!}{w^k (X-1)^{n_x+k}} \Gamma[w(X-1), n_x+k], \quad (44)$$

where n_c and n_x denote the number of co-polar and cross-polar subchannels in the matrix $\mathbf{H}$. For an integer n and a real x, the incomplete gamma function is defined as

$$\Gamma[x, n] = \frac{1}{(n-1)!} \int_0^x t^{n-1} e^{-t} dt. \quad (45)$$

For a complete derivation, we refer the interested reader to Appendix B. We note that

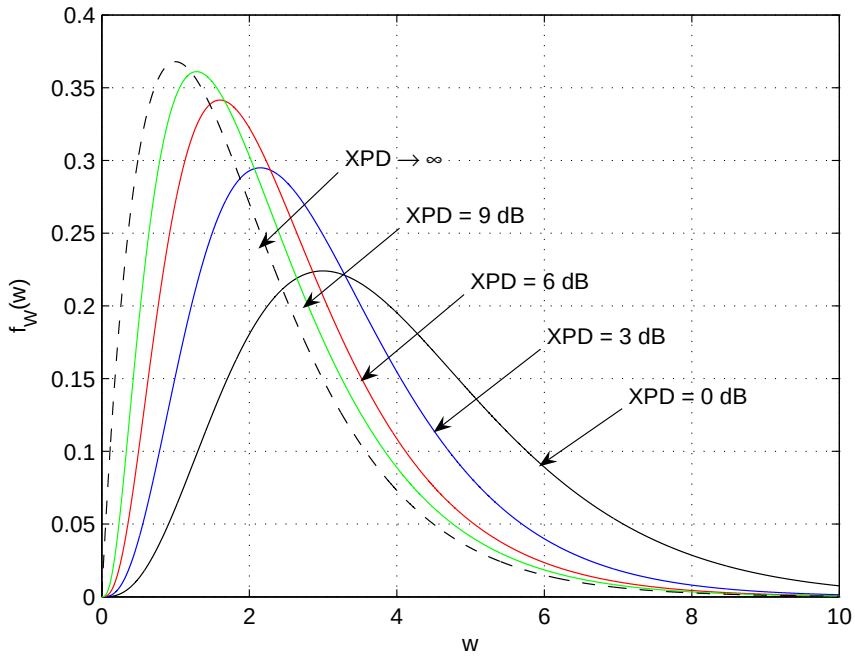

Figure 29: Probability density function of the squared Frobenius norm of a 2×2 dual-polarized MIMO channel for different XPD

for the limiting case ($X \to \infty$), the PDF in equation (44) reduces to equation (43) with $\eta = n_r n_t/2$. Shown in Figure 29, are PDFs of W for a range of values of XPD. It is evident that as the XPD increases, the mean and standard deviation of the random variable W are diminished.

For a given channel $\mathbf{H}$, the bit error rate (BER) of a OSTBC system with Gray mapped 4-QAM constellation is $Pr(\text{error}/\mathbf{H}) = Q(\sqrt{\frac{2WE_b}{N_o}})$ where $E_b/N_o = E_s/(2n_tN_o)$. The average BER can then be calculated as:

$$BER = \int_{-\infty}^{\infty} Q(\sqrt{\frac{wE_s}{n_tN_o}}) f_W(w)dy, \tag{46}$$

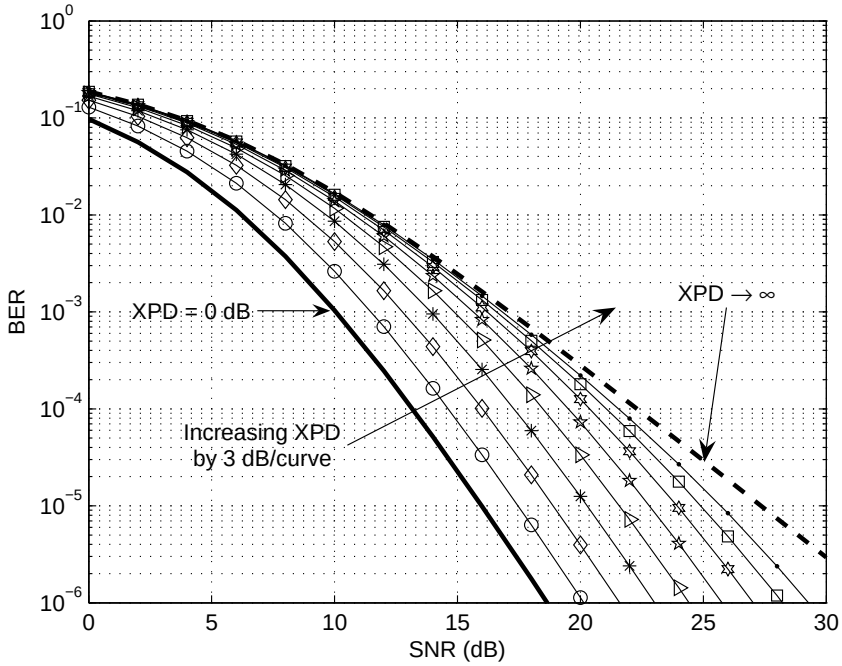

Figure 30: BER performance of Alamouti STBC in dual-polarized MIMO channels for different XPD values

For a spatial MIMO channel, a closed form expression for BER can be developed and it can be shown that at high SNR, $BER \propto \frac{1}{(E_s/N_o)^{\eta}}$ [5]. As mentioned previously, the two extreme cases i.e. $X = 1$ and $X \to \infty$ result in diversity orders $\eta = n_rn_t$ and $\eta = n_rn_t/2$, respectively. However, for other values of X it is not easy to arrive at such insightful approximations. Hence to analyze the influence of XPD on BER, we consider a 2×2 Alamouti space time coded transmission and numerically evaluate (46). As shown in Figure 30, as the XPD increases, BER performance of Alamouti STBC deteriorates. It is interesting to note that even for high XPD, the slope of the BER curve is parallel to $X = 1$ curve.

5.4.2 Norm-based Selection

It is evident from equation (42), that maximizing the channel Frobenius norm maximizes the SNR as well as the instantaneous probability of error for MIMO systems employing OSTBC. Hence for $(n_r, l_r)/(n_t, l_t)$ antenna selection, the selection strategy can be expressed as

$$\widetilde{\mathbf{H}} = arg \min_{S(\bar{\mathbf{H}})} \{\|\bar{\mathbf{H}}\|_F^2\}, \tag{47}$$

where $\bar{\mathbf{H}}$ is obtained by eliminating $n_r - l_r$ columns and $n_t - l_t$ rows from $\mathbf{H}$. $S(\bar{\mathbf{H}})$ denotes the set of all possible $\bar{\mathbf{H}}$. Joint selection at the transmitter and receiver requires a total of $\binom{n_r}{l_r}\binom{n_t}{l_t}$ computations of the Frobenius norm and then a search procedure to find the maximum norm. This computation should not be a problem for practical systems where the number of antennas rarely exceeds four to five. Hence no algorithms have been proposed in the literature to implement this strategy.

To the best of our knowledge, joint selection has not been studied theoretically in the literature, even for spatial MIMO channels. Performance analysis for transmit or receive selection in spatial MIMO channels is provided in [20]. In order to understand the effect of XPD on the selection gain we consider a $(2, 2)/(n_t, l_t)$ system with transmit selection only. Such configurations could be used in WLAN or cellular systems where one end of the link is allowed to be more complex than the other. The analysis is general and is applicable to any OSTBC and can be easily adapted for receive selection.

The selection strategy outlined in equation (47), chooses l_t out of the n_t available transmit antennas to maximize the Frobenius norm of the channel. Let $T_k, k = 1, \ldots, n_t$ denote the squared Frobenius norm of the n_t columns of $\mathbf{H}$. Each column of $\mathbf{H}$ has two independent but non-identical zero mean circularly symmetric complex Gaussian random variables with variances 1 and $1/X$ respectively. They have the probability density functions $g_1(t) = e^{-t}U(t)$ and $g_2(t) = Xe^{-Xt}U(t)$ respectively. The random variables $T_k, k = 1, \ldots, n_t$ are i.i.d random variables with the probability density function given by

$$\begin{aligned} f_T(t) &= g_1(t) * g_2(t) \\ &= \frac{Xe^{-t}}{X-1}(1 - e^{-(X-1)t})U(t) \end{aligned} \tag{48}$$

where, the operator $(*)$ denotes the convolution operation. The cumulative distribution function, can be derived to be

$$\begin{aligned} F_T(t) &= \int_{-\infty}^{t} f_T(x)dx \\ &= \left(1 - \frac{e^{-t}}{X-1}(X - e^{-(X-1)t})\right)U(t) \end{aligned} \tag{49}$$

Invoking the principles of ordered statistics [20], we generate new random variables $T_{[k]}$, $k = 1, \ldots, n_t$ from T_k, $k = 1, \ldots, n_t$ such that

$$T_{[n_t]} \geq T_{[n_t-1]} \geq \ldots \geq T_{[k]} \geq \ldots \geq T_{[2]} \geq T_{[1]}. \tag{50}$$

where $T_{[k]}$ is the k-th largest of the n_t random variables distributed according to (52). Note that these ordered random variables are no longer independent. The average SNR after selection can then be computed as

$$E\{\gamma\} = \gamma_o\Big(E\{T_{[n_t]}\} + E\{T_{[n_t-1]}\} + \ldots + E\{T_{[n_t-l+1]}\}\Big) \tag{51}$$

where $\gamma_o = \frac{E_s}{l_t N o}$.

The probability density function of of the k-th ordered statistic $T_{[k]}$ can then be evaluated as [4],

$$f_k(t) = \frac{n_t!}{(k-1)!(n_t-k)!} F_T(t)^{k-1}(1 - F_T(t))^{n_t-k} f_T(t) \tag{52}$$

The average value of the k-th order statistic can be computed to be

$$E\{T_{[k]}\} = \frac{n_t!}{(k-1)!(n_t-k)!} \sum_{r=0}^{k-1} (-1)^r \binom{k-1}{r} J_{n_t-k+r} \tag{53}$$

where,

$$J_m = \sum_{i=0}^{m} (-1)^i \binom{m}{i} \frac{X^{m-i+1}}{(X-1)^{m+1}} \left[\frac{1}{\big((X-1)i + m + 1\big)^2} - \frac{1}{\big((X-1)(i+1) + m + 1\big)^2}\right] \tag{54}$$

A complete derivation is provided in Appendix C. When $X = 1$, we note that this expression in (53) reduces to [20]

$$E\{T_{[k]}\}_{(X=1)} = \frac{n_t!}{(k-1)!(n_t-k)!} \sum_{r=0}^{k-1} (-1)^r \binom{k-1}{r} \sum_{i=0}^{n_t-k+r} \binom{n_t-k+r}{i} \frac{(2+i)!}{(n_t-k+r+1)^{i+3}}. \tag{55}$$

When $X \to \infty$, the cross-polar subchannels of the $2 \times n_t$ channel matrix $\mathbf{H}$ vanish to zero. As a result each column has one zero element and the other element which is a zero mean unity variance circularly symmetric complex Gaussian random variable. The selection problem in this case reduces to selecting the largest l_t elements out of the n_t non-zero elements in $\mathbf{H}$. The expected value of the k-th order statistic could be derived to be

$$E\{T_{[k]}\}_{(X\to\infty)} = \frac{n_t!}{(k-1)!(n_t-k)!}\sum_{r=0}^{k-1}(-1)^r\binom{k-1}{r}\frac{1}{(n_t+r-k+1)^2} \tag{56}$$

We refer the interested reader to Appendix C for a detailed derivation. In Table 4, we reproduce the average values of the two highest ordered statistics for $l_t = 2$ (Alamouti code), for a range of values of XPD. It is evident that as the XPD increases, the average output SNR decreases.

Table 4: Expected values of the highest and the second highest ordered statistics for different XPD, transmit selection and Alamouti code

	$X = 0$ dB	$X = 3$ dB	$X = 6$ dB	$X = 9$ dB	$X \to \infty$
$n_t = 2$	2.750	2.085	1.776	1.633	1.500
	1.250	0.918	0.726	0.619	0.500
$n_t = 4$	3.547	2.720	2.369	2.218	2.083
	2.210	1.648	1.359	1.217	1.083
$n_t = 6$	4.022	3.105	2.738	2.585	2.450
	2.738	2.059	1.734	1.584	1.450

Performance Analysis

In order to quantitatively measure the performance gain achieved by using antenna selection for dual-polarized MIMO channels, we define the gain metric $G_P(X)$. Note that the average SNR for a $2 \times l_t$ dual-polarized MIMO channe with XPD X is $\gamma_o l_t(1 + 1/X)$. Denoting

$$G_{(n_t,l_t)}(X) = \sum_{k=n_t-l_t+1}^{n_t} E\{T_{[k]}\}, \tag{57}$$

we define $G_P(X)$ as follows

$$G_P(X) = \frac{E\{\gamma\}}{\gamma_o l_t(1+1/X)} = \frac{G_{(n_t,l_t)}(X)}{l_t(1+1/X)} \tag{58}$$

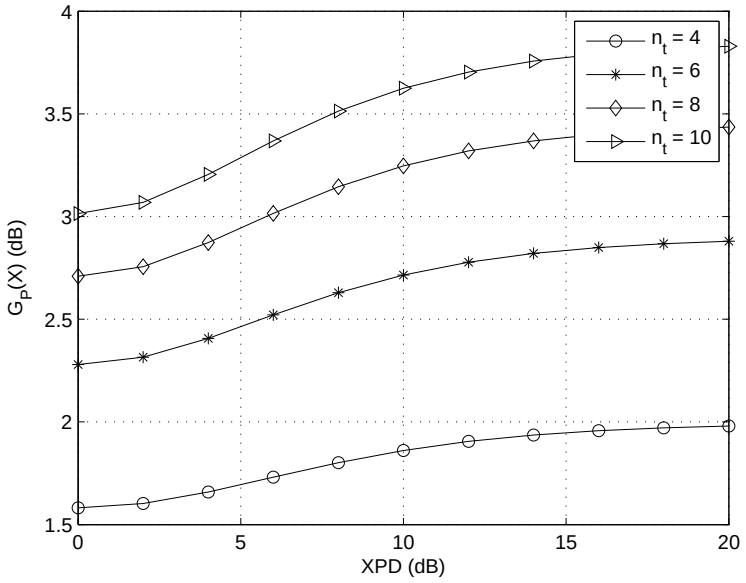

Figure 31: Average SNR gain with (2,2)/(n_t,2) transmit selection for dual-polarized MIMO channels

Shown in Figure 31, are the $G_P(X)$ curves for $(2,2)/(n_t,2)$ transmit selection. It is interesting to note that the gain increases as the XPD increases. Further the gain increases with n_t, but not linearly. The biggest gain is obtained by increasing $n_t = 2$ (no selection) to $n_t = 4$. Increasing the number of transmit antennas from four to six will give much less gain than going from two to four, and in general increasing n_t yields diminishing returns in terms of the SNR gain.

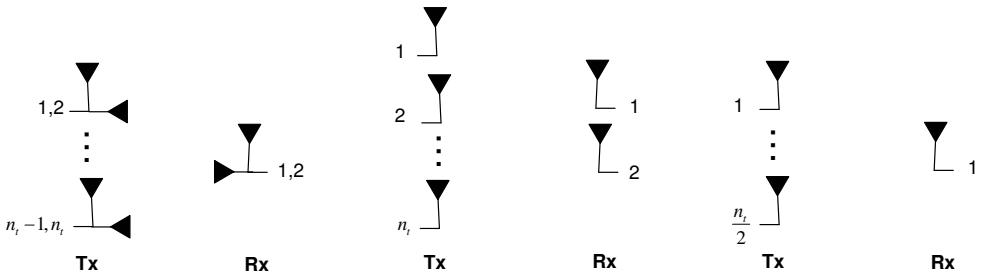

Figure 32: Configurations for evaluation of performance of antenna selection with dual-polarized antennas, over spatial channels. (a) D: $2 \times n_t$ dual-polarized (b) S1: $2 \times n_t$ spatial (c) S2: $1 \times \frac{n_t}{2}$ spatial.

It is imperative to understand the gain (or loss) in performance achieved by antenna

selection for dual-polarized MIMO channels, in comparison with traditional spatial MIMO channels. We note that the constraints of complexity and compactness should be taken into account, to facilitate a fair comparison. We consider a NLOS scenario and assume that the antenna elements are sufficiently separated so that the co-polar subchannels are uncorrelated. The configuration 'D' in Figure 5.4.2 corresponds to the $2 \times n_t$ dual-polarized MIMO configuration being analyzed in this section. The spatial configuration 'S1' has n_t transmit and 2 receive spatially separated uni-polarized antennas. It is reasonable to assume that the realization of this configuration requires a much greater array length at the Tx and the Rx, when compared to the dual-polarized configuration. The second spatial configuration 'S2' has $n_t/2$ transmit and one receive uni-polarized antennas. This configuration has a similar form factor as 'D' and it is assumed that $n_t > 2l_t$. All the elements of the spatial MIMO channels 'S1' and 'S2' can be assumed to be i.i.d Rayleigh with unity variance. Further we remind the reader that $X = 1$ corresponds to the spatial case and hence all the results developed so far are applicable to these spatial configurations.

We define the first metric $G_{S1}(X)$ to provide a measure of the loss in performance of $(2,2)/(n_t,l_t)$ antenna selection, incurred by using dual-polarized antennas for the sake of compactness, instead of the spatial configuration 'S1'. It is defined as

$$G_{S1}(X) = \frac{G_{(n_t,l_t)}(X)}{G_{(n_t,l_t)}(1)} \tag{59}$$

In addition to providing compactness, dual-polarized antennas could be used to realize higher order MIMO architectures in compact devices. We define the metric $G_{S2}(X)$ to provide a measure of performance improvement resulting from the use of antenna selection with the higher order dual-polarized configuration 'D' instead of the uni-polarized spatial configuration 'S2'. Note that 'S2' uses only one RF chain at the receiver. Hence for a fair comparison, $(2,1)/(n_t,l_t)$ selection must be implemented for the configuration 'D'. The gain metric $G_{S2}(X)$ is defined as

$$G_{S2}(X) = \frac{\gamma_D(X)}{\gamma_{S2}(X)}, \tag{60}$$

where $\gamma_D(X)$ and $\gamma_{S2}(X)$ are the average SNR of the $(2,1)/(n_t,l_t)$ dual-polarized configuration and $(1,1)/(n_t/2,l_t)$ spatial configuration 'S2' respectively. Since the theoretical

analysis in this section is limited to selection at one end, we evaluate $G_{S2}(X)$ through simulations.

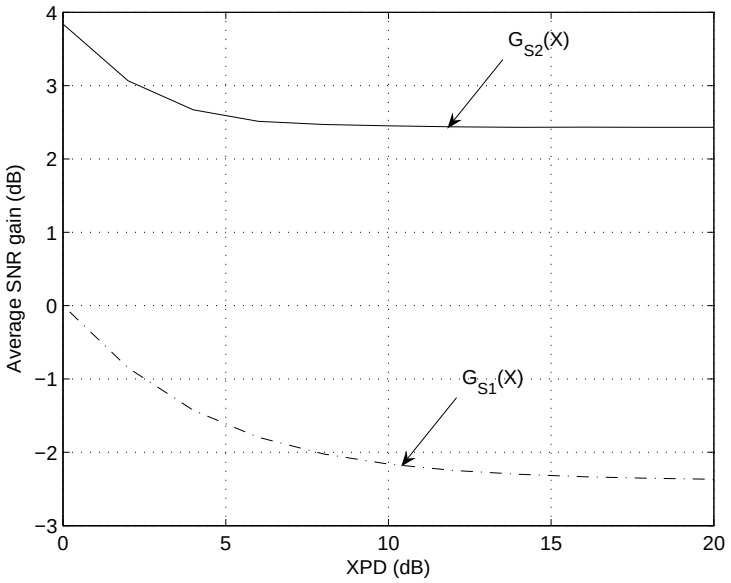

Figure 33: Performance of antenna selection with dual-polarized antennas with respect to spatial configurations S1 and S2; $n_t = 6$ and $l_t = 2$.

Shown in Figure 33, are the $G_{S1}(X)$ and $G_{S2}(X)$ curves for $n_t = 6$ and $l_t = 2$. It is evident from the $G_{S1}(X)$ curve that the performance of antenna selection with dual-polarized antennas is significantly diminished at high XPD, when compared to the spatial MIMO configuration 'S1', with a larger form factor. Thus we contend that when space is not a constraint, spatial MIMO should be preferred over dual-polarized MIMO. On the other hand when dual-polarized and spatial configurations with similar form factors and complexity are compared, antenna selection for the former configuration performs much better than the latter even at high XPD. Hence antenna selection combined with dual-polarized antennas present an attractive alternative, to realize higher order MIMO architectures in compact devices.

5.4.3 Measured BER Results

It is important to understand the performance of antenna selection for dual-polarized MIMO channels in relation to traditional spatial MIMO channels. In this section we study the performance of antenna selection for both spatial and dual-polarized MIMO systems employing OSTBC. We use the normalized measured channel samples to achieve this objective. The input symbols s_i were drawn from an equiprobable 4-QAM constellation $\{\pm 1 \pm j\}/\sqrt{2}$. The channel was assumed to be static for a frame of 100 symbols. BER is calculated for each frame and averaged over the N channel realizations provided by the measurements (See Table 4.1). The array length is the same at the Tx and the Rx. Although we have theoretically studied antenna selection for one end of the link, we maintain that selection could be easily implemented at both ends with the availability of a perfect low bandwidth feedback channel. Hence in this section, we consider (4,2)/(4,2) optimal antenna selection according to the criteria outlined in (47), for an Alamouti space time coded system, under LOS and NLOS channel conditions, for a range of values of inter-element spacing. We use exhaustive search to achieve optimal selection.

In Figures 34(a) and 34(b), we plot the BER curves for (4,2)/(4,2) selection under LOS and NLOS channel conditions respectively. In these figures, we consider a 4×4 dual-polarized system with $L \in \{\lambda/2, \lambda, 3\lambda/2\}$ and a spatial system with $L = 3\lambda/2$. The minimum inter-element spacing between the adjacent antenna elements is maintained at $\lambda/2$. For reference we also plot the BER for deterministic selection (DS) for 2×2 spatial MIMO with $L \in \{\lambda/2, \lambda, 3\lambda/2\}$.

In the hallway, as the inter-element spacing is increased, the performance of the 2×2 spatial MIMO with deterministic selection improves owing to the decrease in the subchannel correlations and the spherical wavefront effect [26]. Further the performance of the 4×4 dual-polarized MIMO with selection also improves with increasing inter-element spacing because of the lower correlations between the elements of the co-polar submatrices $\mathbf{H}^{VV}$ and $\mathbf{H}^{HH}$. For an array length of $L = \lambda/2$, the $(4,2)/(4,2)$ dual-polarized MIMO system outperforms the deterministic 2×2 spatial MIMO with the same array length by about 2.7 dB at BER $= 10^{-2}$. On the other hand, the $(4,2)/(4,2)$ spatial system with $L = 3\lambda/2$

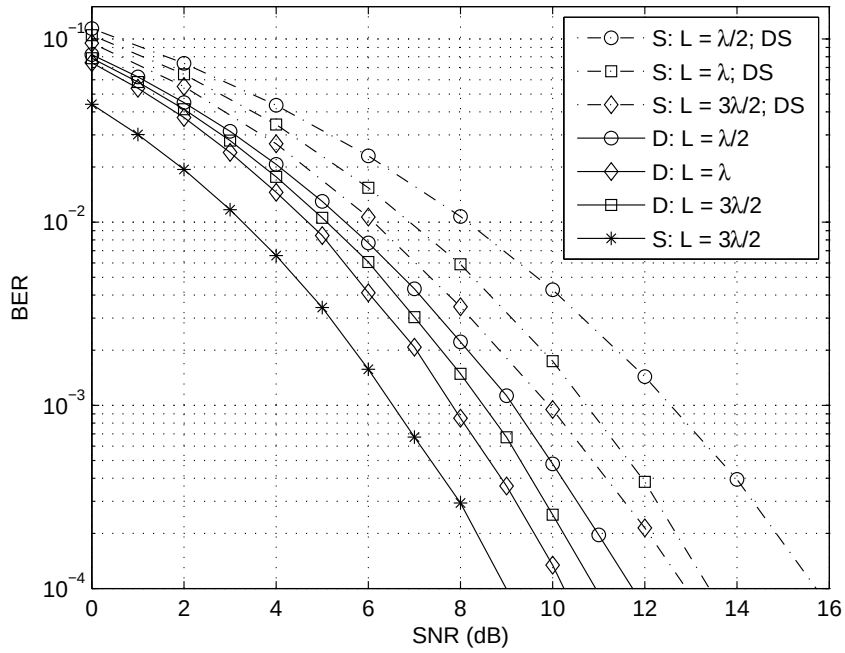

(a)

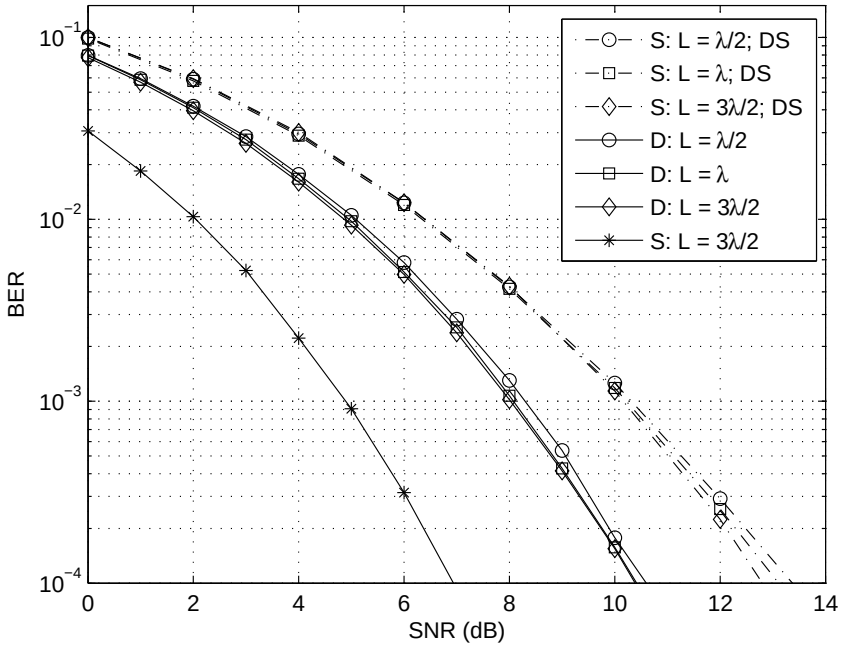

(b)

Figure 34: Measured BER for (4,2)/(4,2) antenna selection with Alamouti STBC under (a) LOS and (b) NLOS channel conditions

outperforms its dual-polarized counterpart by about 2 dB at BER = 10^{-2}.

Under NLOS channel conditions, as expected, the performance is not a strong function of the inter-element spacing. For $L = \lambda/2$, the 4×4 dual-polarized system with selection outperforms the 2×2 deterministic spatial MIMO by just under 1.5 dB at BER = 10^{-2}. The (4,2)/(4,2) spatial MIMO with $L = 3\lambda/2$ outperforms the dual-polarized MIMO with selection by about 3 dB.

We end this chapter with an important observation. The gains achieved by antenna selection for MIMO systems employing OSTBC are lower than for spatial multiplexing systems. In a multiplexing system with linear receiver processing, some of the degrees of diversity are expended in suppressing the interfering data streams. As a result the system achieves a diversity order of only $n_r - n_t + 1$. On the other hand, in OSTBC systems, all the $n_r n_t$ degrees of diversity are allocated to a single data stream. It is well known that we achieve diminishing returns in performance as the degrees of diversity are increased [5]. Hence antenna selection, which basically provides additional degrees of diversity is more effective for spatial multiplexing systems when compared to MIMO systems employing OSTBC.

CHAPTER VI

CONCLUSIONS AND FUTURE WORK

This chapter summarizes the contributions of this thesis and suggests some possible research areas for future work.

Research Contributions

This thesis deals with dual-polarized MIMO channels, an important topic for the practical deployment of MIMO architectures in compact devices. The following are the major contributions of this work.

1. This thesis provides a complete set of indoor MIMO channel measurements using dual-polarized antennas at 2.4 GHz. Analysis presented herein highlights the differences between dual-polarized and traditional spatial MIMO configurations, in terms of channel characteristics and achievable capacity [3].

2. It presents a tight analytical lower bound, for the ergodic capacity of 2×2 dual-polarized Ricean and Rayleigh MIMO channels, in terms of the channel parameters.

3. This thesis is the first to explore the possibility of using antenna selection for compact dual-polarized MIMO systems. Using theoretical analysis and measurement results, it provides a comprehensive performance analysis of antenna selection for dual-polarized MIMO systems employing VBLAST or STBC.

The current trend of miniaturization seems to be at odds with the implementation of spatial MIMO architectures in compact wireless devices, such as handheld and notebook computers, mobile phones, music players and wireless sensors. The results presented in this thesis, illustrate that dual-polarized antennas provide an attractive solution to the problem of realizing higher order MIMO configurations in these devices. Furthermore, this thesis motivates the use of antenna selection combined with dual-polarized antennas for compact

devices, which are often constrained by complexity, power and costs. Thus the benefits of the MIMO architecture could be reaped, with only a nominal increase in complexity and with no expense in terms of space.

Future Work

Unlike spatial MIMO channels, dual-polarized MIMO channels have not been extensively studied in the literature. This thesis addresses a few issues related to this topic. However, there remain many important issues that need to be resolved, before these configurations can be deployed in future wireless devices.

- *Extensive Measurements and Simulation Models*: The measurements provided in our thesis are limited to two typical scenarios in indoor environments. We emphasize that more comprehensive measurements, in a wide range of channels, are needed to accurately model dual-polarized MIMO channels. To the best of our knowledge there exists no simulation model for 4×4 or higher order MIMO channels. Simulation models are important, as they will enable system designers to simulate and evaluate the performance of these systems under harsh radio propagation conditions.

- *Wideband Channels*: This thesis has dealt with only flat fading channels. However, future wireless systems will employ wideband communication channels to deliver higher data rates. Hence it is imperative to understand the characteristics and performance of dual-polarized MIMO channels in the presence of frequency selective fading.

- *Keyhole Channels*: Recently, in multiple-input multiple-output (MIMO) fading environments, the existence of rank-deficient channels called keyhole channels has been demonstrated [9]. In such scenarios, the spatial MIMO matrix is unity rank and hence achieves similar spectral efficiency as a SISO channel. We envisage that by using dual-polarized antennas in such channels, the rank of the channel matrix can at least be increased to two. This indicates a huge potential for performance improvement in keyhole channels and hence warrants further study.

APPENDIX A

DERIVATION OF EQUATIONS 23 AND 24

We first restate the assumptions made in Section 3.4.2, with a slight change in notation. Consider a 2×2 dual-polarized MIMO channel matrix $\mathbf{H} = \{h_{ij}\}$ $1 \leq i, j \leq 2$. We make the simplifying assumption that $X_V = X_H = 1/\alpha$, $0 \leq \alpha \leq 1$. All the channel entries are assumed to be mutually independent circularly symmetric complex Gaussian random variables with the following variances

$$\begin{array}{llll} E\{|h_{11}|^2\} & = 1; & E\{|h_{12}|^2\} & = \beta\alpha \\ E\{|h_{21}|^2\} & = \alpha; & E\{|h_{22}|^2\} & = \beta. \end{array} \tag{61}$$

and the following means

$$\begin{array}{llll} E\{h_{11}\} & = \sqrt{\frac{K}{K+1}}; & E\{h_{12}\} & = 0 \\ E\{h_{21}\} & = 0; & E\{h_{22}\} & = \sqrt{\frac{\beta K}{K+1}}. \end{array} \tag{62}$$

Here $K_{VV} = K_{HH} = K$ is the K factor corresponding to the co-polar subchannels. For a real gaussian random variable Z with mean μ and variance σ^2, $E\{Z^4\} = \mu^4 + 6\mu^2\sigma^2 + 3\sigma^4$. Using this fact, the fourth order moment of the absolute value of a circularly symmetric complex Gaussian random variable can be calculated. The fourth order moments of the subchannel entries can be easily evaluated to be

$$\begin{array}{llll} E\{|h_{11}|^4\} & = 1 + \frac{2K+1}{(K+1)^2}; & E\{|h_{12}|^4\} & = 2\beta^2\alpha^2 \\ E\{|h_{21}|^4\} & = 2\alpha^2; & E\{|h_{22}|^4\} & = \beta^2\big(1 + \frac{2K+1}{(K+1)^2}\big) \end{array} \tag{63}$$

Now consider the symmetric matrix

$$\begin{aligned} \mathbf{W} &= \mathbf{H}\mathbf{H}^H \\ &= \begin{bmatrix} |h_{11}|^2 + |h_{12}|^2 & h_{11}h_{21}^* + h_{12}h_{22}^* \\ h_{11}^*h_{21} + h_{12}^*h_{22} & |h_{21}|^2 + |h_{22}|^2 \end{bmatrix}. \end{aligned} \tag{64}$$

It is easy to see from (61) that the mean values of the elements of this matrix are given by

$$\begin{array}{llll} E\{w_{11}\} & = 1 + \beta\alpha; & E\{w_{12}\} & = 0 \\ E\{w_{21}\} & = 0; & E\{w_{22}\} & = \alpha + \beta. \end{array} \tag{65}$$

Note that w_{11} and w_{22} are independent random variables. The values $E\{|w_{11}|^2\}$ and $E\{|w_{22}|^2\}$ will be required in our calculations. Hence we proceed to calculate these values as follows

$$\begin{aligned} E\{|w_{11}|^2\} &= E\{(|h_{11}|^4 + |h_{12}|^4 + 2|h_{11}|^2|h_{12}|^2)\} \\ &= 1 + \frac{2K+1}{(K+1)^2} + 2\beta^2\alpha^2 + 2\beta\alpha \end{aligned} \tag{66}$$

Similarly,

$$\begin{aligned} E\{|w_{22}|^2\} &= E\{(|h_{22}|^4 + |h_{21}|^4 + 2|h_{22}|^2|h_{21}|^2)\} \\ &= \beta^2\left(1 + \frac{2K+1}{(K+1)^2}\right) + 2\alpha^2 + 2\beta\alpha \end{aligned} \tag{67}$$

Denoting $D = E\{\det(\mathbf{I}_2 + \frac{\rho}{2}\mathbf{W})\}$, the expression for the lower bound of ergodic capacity of channel $\mathbf{H}$ is given by (22),

$$\bar{C}(\rho) \geq \log_2(E\{D\}) - \frac{\log_2(e)}{2}\frac{E\{D^2\} - (E\{D\})^2}{(E\{D\})^2} \tag{68}$$

Thus we need to evaluate $E\{D\}$ and $E\{D^2\}$ using the statistics of the entries of the matrix $\mathbf{W}$ computed above. $E\{D\}$ can be derived as follows

$$\begin{aligned} E\{D\} &= E\{1 + \frac{\rho}{2}(w_{11} + w_{22}) + \frac{\rho^2}{4}(w_{11}w_{22} - w_{12}w_{21})\} \\ &= 1 + \frac{\rho}{2}E\{(w_{11} + w_{22})\} + \frac{\rho^2}{4}E\{|h_{11}|^2|h_{22}|^2 + |h_{12}|^2|h_{21}|^2\} \\ &= 1 + \frac{\rho}{2}(1+\alpha)(1+\beta) + \frac{\rho^2}{4}\beta(1+\alpha^2), \end{aligned} \tag{69}$$

Now $E\{D^2\}$ is given by,

$$\begin{aligned} E\{D^2\} &= 1 + \rho\underbrace{E\{w_{11} + w_{22}\}}_{A_1} + \frac{\rho^2}{4}\underbrace{E\{w_{11}^2 + w_{22}^2 + 4w_{11}w_{22} - 2w_{12}w_{21}\}}_{A_2} \\ &\quad + \frac{\rho^3}{4}\underbrace{E\{w_{11}^2w_{22} + w_{22}^2w_{11} - w_{21}w_{12}(w_{11} + w_{22})\}}_{A_3} \\ &\quad + \frac{\rho^4}{16}\underbrace{E\{(w_{11}w_{22} - w_{12}w_{21})^2\}}_{A_4} \end{aligned} \tag{70}$$

We compute each of the terms in the above expression individually. Using (65),(66) and (67), terms A_1 and A_2 can be evaluated to be

$$A_1 = (1+\beta)(1+\alpha) \tag{71}$$

and

$$A_2 = 2(2(1+\alpha^2+\alpha)(1+\beta)^2 + \bar{K}(1+\beta^2)) \tag{72}$$

where, $\bar{K} = -K^2/(K+1)^2$. Now to compute A_3, we need the following values

$$\begin{aligned} E\{w_{21}w_{12}w_{11}\} &= E\Big\{|h_{11}|^4|h_{21}|^2 + |h_{22}|^2|h_{12}|^4 + |h_{11}|^2|h_{22}|^2|h_{12}|^2 + |h_{11}|^2|h_{21}|^2|h_{12}|^2\Big\} \\ &= \alpha\left(1+\frac{2K+1}{(K+1)^2}\right) + 2\beta^3\alpha^2 + \beta^2\alpha + \beta\alpha^2, \end{aligned}$$

and similarly

$$\begin{aligned} E\{w_{21}w_{12}w_{22}\} &= E\Big\{|h_{22}|^4|h_{12}|^2 + |h_{11}|^2|h_{21}|^4 + |h_{11}|^2|h_{21}|^2|h_{22}|^2 + |h_{22}|^2|h_{21}|^2|h_{12}|^2\Big\} \\ &= \beta^3\alpha\left(1+\frac{2K+1}{(K+1)^2}\right) + 2\alpha^2 + \beta\alpha + \beta^2\alpha^2. \end{aligned}$$

Then, A_3 can be shown to be

$$A_3 = \beta(1+\beta)((1+\alpha)(2\alpha^2-\alpha+2) + \bar{K}) \tag{73}$$

The final term A_4 can be computed as follows,

$$\begin{aligned} A_4 &= E\{(w_{11}w_{22} - w_{12}w_{21})^2\} \\ &= E\Big\{(|h_{11}|^2|h_{22}|^2 + |h_{12}|^2|h_{21}|^2 - h_{11}h_{21}^*h_{22}h_{12}^* - h_{11}^*h_{21}h_{22}^*h_{12})^2\Big\} \\ &= E\{|h_{11}|^4|h_{22}|^4\} + E\{|h_{12}|^4|h_{21}|^4\} + 4E\{|h_{11}|^2|h_{12}|^2|h_{21}|^2|h_{22}|^2\} \\ &= \left(1+\frac{2K+1}{(K+1)^2}\right)^2\beta^2 + 4\alpha^4\beta^2 + 4\alpha^2\beta^2. \end{aligned} \tag{74}$$

Plugging these terms into equation (70) yields the desired equation in (24).

APPENDIX B

DERIVATION OF EQUATION 44

Assume that $X_V = X_H = X$ and $\beta = 1$. We assume that all the elements of the $n_r \times n_t$ channel matrix $\mathbf{H}$ are independent and zero mean circularly symmetric complex Gaussian random variables. The co-polar subchannels have unity variance while the cross-polar subchannels have a variance $1/X$. The squared Frobenius norm of the $n_r \times n_t$ channel matrix $\mathbf{H}$ can be written as

$$\begin{aligned} W &= (\|\mathbf{H}^{VV}\|^2 + \|\mathbf{H}^{HH}\|^2) + (\|\mathbf{H}^{VH}\|^2 + \|\mathbf{H}^{HV}\|^2) \\ &= W_c + W_x. \end{aligned} \tag{75}$$

The random variables W_c and W_x correspond to the co-polar and cross-polar submatrices of the channel. They are independent but not identically distributed. W_c is a chi-squared random variable with $n_c = n_r^V n_t^V + n_r^H n_t^H$ degrees of freedom and with a probability density function,

$$f_{W_c}(w) = \frac{w^{n_c-1}e^{-w}}{(n_c-1)!}U(w) \tag{76}$$

Now using the fact that $W_x = \frac{W_c}{X}$, the probability density function of W_x can be easily computed to be

$$f_{W_x}(w) = \frac{X^{n_x}w^{n_x-1}e^{-wX}}{(n_x-1)!}U(w), \tag{77}$$

where $n_x = n_r^V n_t^H + n_r^H n_t^V$. Since W_c and W_x are independent random variables, the probability density function of W is given by

$$
\begin{aligned}
f_W(w) &= f_{W_c}(w) * f_{W_x}(w) \\
&= \int_{-\infty}^{\infty} f_{W_c}(w-t) f_{W_x}(t) dt \\
&= \frac{X^{n_x} e^{-w} w^{(n_c-1)}}{(n_c-1)(n_x-1)} \int_0^w t^{(n_x-1)} \left(1 - \frac{t}{w}\right)^{n_c-1} e^{-t(X-1)} dt \\
&= C \int_0^w \sum_{k=0}^{n_c-1} \frac{(-1)^k}{w^k} \binom{n_c-1}{k} t^{(n_x+k-1)} e^{-t(X-1)} dt \\
&= C \sum_{k=0}^{n_c-1} \frac{(-1)^k}{w^k} \binom{n_c-1}{k} \int_0^w t^{(n_x+k-1)} e^{-t(X-1)} dt \\
&= C \sum_{k=0}^{n_c-1} \binom{n_c-1}{k} \frac{(-1)^k (n_x+k-1)!}{w^k (X-1)^{n_x+k}} \Gamma[w(X-1), n_x+k], \qquad (78)
\end{aligned}
$$

where the operator $(*)$ denotes the convolution operation, $C = \frac{X^{n_x} e^{-w} w^{(n_c-1)}}{(n_c-1)(n_x-1)}$ and $\Gamma[x,n]$ is the incomplete Gamma function given by

$$\Gamma[x,n] = \frac{1}{(n-1)!} \int_0^x t^{n-1} e^{-t} dt.$$

APPENDIX C

DERIVATION OF EQUATION 53

From (51), the average SNR of a $(2,2)/(n,l)$ selection is given by,

$$E\{\gamma\} = \gamma_o\Big(E\{T_{[n]}\} + E\{T_{[n-1]}\} + \ldots + E\{T_{[n-l+1]}\}\Big)$$

where, the random variables $T_{[k]}$, $k = 1, \ldots, n$ have been defined earlier. Essentially we are interested in the first order moments of $T_{[k]}$, $k = 1, \ldots, l$. The probability density function of of the k-th ordered statistic $T_{[k]}$ can then be evaluated as,

$$f_k(t) = \frac{n!}{(k-1)!(n-k)!} F_T(t)^{k-1}(1 - F_T(t))^{n-k} f_T(t)$$

where

$$f_T(t) = \frac{Xe^{-t}}{X-1}(1 - e^{-(X-1)t})U(t)$$

and the cumulative distribution function given by

$$F_T(t) = \left(1 - \frac{e^{-t}}{X-1}(X - e^{-(X-1)t})\right)U(t)$$

We have

$$\begin{aligned} E\{T_{[k]}\} &= \frac{n!}{(k-1)!(n-k)!} \int_{-\infty}^{\infty} t F_T(t)^{k-1}(1 - F_T(t))^{n-k} f_T(t) dt \\ &= \frac{n!}{(k-1)!(n-k)!} \sum_{r=0}^{k-1} (-1)^r \binom{k-1}{r} \int_{-\infty}^{\infty} t(1 - F_T(t))^{n-k+r} f_T(t) dt \\ &= \frac{n!}{(k-1)!(n-k)!} \sum_{r=0}^{k-1} (-1)^r \binom{k-1}{r} J_{n-k+r} \end{aligned}$$

where for an integer m

$$
\begin{aligned}
J_m &= \int_{-\infty}^{\infty} t(1-F_T(t))^m f_T(t)dt \\
&= \int_0^{\infty} t\left(\frac{e^{-t}}{X-1}(X-e^{-(X-1)t})\right)^m \frac{Xe^{-t}}{X-1}(1-e^{-(X-1)t})dt \\
&= \frac{X^{m+1}}{(X-1)^{m+1}}\int_0^{\infty} te^{-(m+1)t}\left(1-\frac{e^{-(X-1)t}}{X}\right)^m (1-e^{-(X-1)t})dt \\
&= \frac{X^{m+1}}{(X-1)^{m+1}}\int_0^{\infty} te^{-(m+1)t}\left(\sum_{i=0}^{m}(-1)^i\binom{m}{i}\frac{e^{-(X-1)it}}{X^i}\right)(1-e^{-(X-1)t})dt \\
&= \frac{X^{m+1}}{(X-1)^{m+1}}\sum_{i=0}^{m}\frac{(-1)^i}{X^i}\left[\int_0^{\infty} te^{-\left((m+1)+(X-1)i\right)t}dt - \int_0^{\infty} te^{-\left((m+1)+(X-1)(i+1)\right)t}dt\right] \\
&= \sum_{i=0}^{m}(-1)^i\binom{m}{i}\frac{X^{m-i+1}}{(X-1)^{m+1}}\left[\frac{1}{((X-1)i+m+1)^2} - \frac{1}{((X-1)(i+1)+m+1)^2}\right]
\end{aligned}
$$

Limiting Cases

Now we consider the special cases of $X \downarrow 1$ and $X \to \infty$. We show that in these cases (53) reduces to (56) and (55) respectively. The problem is to find

$$(a)\lim_{X\downarrow 1}\int_0^{\infty} tf_k(t)dt$$

and

$$(b)\lim_{X\to\infty}\int_0^{\infty} tf_k(t)dt$$

We first look at part (a). Invoking the Dominated Convergence Theorem [50], it can be shown that

$$\lim_{X\downarrow 1}\int_0^{\infty} tf_k(t)dt = \int_0^{\infty} t\left(\lim_{X\downarrow 1} f_k(t)\right)dt$$

And it is easy to see that $f(t) = \lim_{X\downarrow 1} f_T(t) = te^{-t}U(t)$ and $F(t) = \lim_{X\downarrow 1} F_T(t) = (1-e^{-t}-te^{-t})U(t)$. It follows that

$$g(t) = \lim_{X\downarrow 1} f_k(t) = CF(t)^{k-1}(1-F(t))^{n-k}f(t).$$

where $C = \frac{n!}{(k-1)!(n-k)!}$. Expanding $F(t)^{k-1} = (1 - e^{-t} - te^{-t})^{k-1}$ into a binomial series, we get

$$\begin{aligned}
\int_0^\infty tg(t)dt &= C\int_0^\infty tF(t)^{k-1}(1-F(t))^{n-k}f(t)dt \\
&= C\sum_{r=0}^{k-1}(-1)^r\binom{k-1}{r}\int_0^\infty (1+t)^{n-k+r}e^{-(n-k+r+1)t}t^2dt \\
&= C\sum_{r=0}^{k-1}(-1)^r\binom{k-1}{r}\sum_{i=0}^{n-k+r}\binom{n-k+r}{i}\int_0^\infty e^{-(n-k+r+1)t}t^{i+2}dt
\end{aligned}$$

Using the fact that $\int_0^\infty x^n e^{-ax}dx = n!/a^{n+1}$, we get the desired result in equation (55).

For part (b), a similar analysis follows by observing that $f(t) = \lim_{X\to\infty} f_T(t) = e^{-t}U(t)$ and $F(t) = \lim_{X\to\infty} F_T(t) = (1 - e^{-t})U(t)$.

REFERENCES

[1] Abdi, A., Tepedelenlioglu, C., Kaveh, M., and Giannikis, G., "On the estimation of the K parameter for the Rice fading distribution," *IEEE Communication Letters*, vol. 5, March 2001.

[2] Alamouti, S., "A simple transmit diversity technique for wireless communications," *IEEE Journal on Selected Areas in Communications*, vol. 16, pp. 1451 – 1458, Oct 1998.

[3] Anreddy, V. and Ingram, M., "Capacity of measured Ricean and Rayleigh indoor MIMO channels at 2.4 GHz with polarization and spatial diversity," *IEEE Wireless Communications and Networking Conference*, 2006.

[4] Balakrishnan, N. and Cohen, A., *Order Statistics and Inference: Estimation Methods*. Academic Press Inc., 2nd ed., 1991.

[5] Barry, J., Lee, E., and Messerschmitt, D., *Digital Communication*. Kluwer Academic Publishers, 2nd ed., 2001.

[6] Berenguer, I., Wang, X., and Wassell, I., "Antenna selection in linear receivers: Geometrical approach," *IEE Electronic Letters*, vol. 40, pp. 292–293, March 2004.

[7] Berenguer, I., Wang, X., and Krishnamurthy, V., "Adaptive MIMO antenna selection via discrete stochastic optimization," *IEEE Transactions on Signal Processing*, vol. 53, pp. 4315 – 4329, Nov 2005.

[8] Blum, R. and Winters, J., "On optimum MIMO with antenna selection," *Communications Letters, IEEE*, vol. 6, pp. 322–324, Aug 2002.

[9] Chizhik, D., Foschini, G., Gans, M., and Valenzuela, R., "Keyholes, correlations, and capacities of multielement transmit and receive antennas," *IEEE Transactions on Wireless Communications,*, vol. 1, pp. 361–368, April 2002.

[10] Deng, Y., Burr, A., and White, G., "Performance of MIMO systems with combined polarization multiplexing and transmit diversity," *IEEE Vehicular Technology Conference*, vol. 2, pp. 869–873, May 2005.

[11] Erceg, V., Soma, P., Baum, D., and Catreux, S., "Multiple-input multiple-output fixed wireless radio channel measurements and modelling using dual-polarized antennas at 2.5 GHz," *IEEE Transactions on Wireless Communications*, vol. 3, pp. 2288–2298, Nov. 2004.

[12] Foschini, G., "Layered space-time architecture for wirless communication in a fading environment when using multi-element antennas," *Bell Labs Technical Journal*, pp. 41–59, Autumn 1996.

[13] Foschini, G. and Gans, M., "On limits of wireless communications in a fading environment when using multiple antennas," *Wireless Personal Communications*, vol. 6, p. 311335, 1998.

[14] Gaur, S. and Ingram, M. A., "Transmit/receive antenna selection for MIMO systems to improve error performance of linear receivers," *Proceedings of International ITG/IEEE Workshop on Smart Antennas*, April 2005.

[15] Gesbert, D., Shafi, M., Shiu, A., Smith, P., and Naguib, A., "From theory to practice: An overview of MIMO space-time coded wireless systems," *IEEE Journal on selected areas in Communications*, vol. 21, pp. 281–301, April 2003.

[16] Gharavi-Alkhansari, M. and Gershman, A., "Fast antenna subset selection in wireless MIMO systems," *IEEE International Conference on Acoustics, Speech, and Signal Processing*, vol. 5, pp. 57–60, 2003.

[17] Godavarti, M., Marzetta, T., and Shamai, S., "Capacity of mobile multiple-antenna wireless link with isotropically random Rician fading," *IEEE ISIT*, June 2001.

[18] Gore, D., Nabar, R., and Paulraj, A., "Selecting an optimal set of transmit antennas for a low rank matrix channel," *IEEE Internation Conference on Acoustics, Speech and Signal Processing*, June 2000.

[19] Gore, D. A., Heath, R. W., and Paulraj, A., "Transmit selection in spatial multiplexing systems," *IEEE Communications Letters*, vol. 6, pp. 491–493, Nov 2002.

[20] Gore, D. and Paulraj, A., "MIMO antenna subset selection with space-time coding," *IEEE Transactions on Signal Processing*, vol. 50, pp. 2580 – 2588, Oct 2002.

[21] Gorokhov, A., Gore, D., and Paulraj, A., "Receive antenna selection for MIMO flat-fading channels: theory and algorithms," *IEEE Transactions on Information Theory*, vol. 49, pp. 2687–2696, Oct 2003.

[22] Hashemi, H., "The indoor radio propagation channel," *Proceedings of IEEE*, vol. 81, pp. 943 – 968, July 1993.

[23] Jagannatham, A. and Erceg, V., "MIMO indoor WLAN channel measurements and parameter modeling at 5.25 GHz," *IEEE Vehicular Technology Conference*, vol. 1, pp. 106 – 110, Sept 2004.

[24] Janaswamy, R., "Effect of element mutual coupling on the capacity of fixed linear arrays," *IEEE Antennas and Wireless Propagation Letters*, vol. 1, no. 1, pp. 157–160, 2002.

[25] Jiang, J., *Measurement, Modeling, and Performance of indoor MIMO channels*. PhD thesis, Georgia Institute of Technology, Atlanta, GA, USA, May 2004.

[26] Jiang, J. and Ingram, M., "Spherical-wave model for short-range MIMO," *IEEE Transactions on Communications*, vol. 53, pp. 1534 – 1541, Sept. 2005.

[27] Jootar, J. and Zeidler, J., "Performance analysis of polarization receive diversity in correlated rayleigh fading channels," *IEEE Global Telecommunications Conference*, vol. 2, pp. 774 – 778, 2003.

[28] Kermoal, J., Schumacher, L., Frederiksen, F., and Mogensen, P., "Polarization diversity in MIMO radio channels: Experimental validation of a stochastic model. and performance assessment," *IEEE Vehicular Technology Conference*, vol. 1, pp. 22–26, Oct. 2001.

[29] Kermoal, J., Schumacher, L., Pedersen, K., Mogensen, P., and Frederiksen, F., "A stochastic MIMO radio channel model with experimental validation," *IEEE Journal on Selected Areas in Communication*, vol. 20, pp. 1211–1226, Aug. 2002.

[30] Kyritsi, P., "K factor estimation in a hallway using waveguide mode analysis," *COST 273, Management Committee meeting*, January 2002.

[31] Kyritsi, P., Cox, D., Valenzuela, R., and P.W, W., "Effect of antenna polarization on the capacity of a multiple element system in an indoor environment," *IEEE Journal on Selected areas in Communications*, vol. 20, pp. 1227–1239, Aug. 2002.

[32] Kyritsi, P., Cox, D., Valenzuela, R., and P.W, W., "Correlation analysis based on MIMO channel measurements in an indoor environment," *IEEE Journal on Selected Areas In Communications*, vol. 21, pp. 713–720, June 2003.

[33] Kyritsi, P. and D.C., C., "Propagation characteristics of horizontally and vertically polarized electric fields in an indoor environment: simple model and results," *IEEE Vehicular Technology Conference*, vol. 3, pp. 1422–1426, Oct. 2001.

[34] Li, H. J. and Yu, C., H., "MIMO channel capacity for various polarization combinations," *Journal of Electromagnetics, Waves and Applications*, vol. 18, pp. 301–320, March 2004.

[35] Maleki, N., Karami, E., and Shiva, M., "The effect of array length on the capacity of MIMO channels," *IEEE International Signal Processing and Information Technology Conference*, pp. 17–21, Dec 2004.

[36] Molisch, A. and Win, M., "MIMO systems with antenna selection," *IEEE Microwave Magazine*, vol. 5, pp. 46 – 56, March 2004.

[37] Molisch, A.F.and Win, M., Choi, Y.-S., and Winters, J., "Capacity of MIMO systems with antenna selection," *IEEE Transactions on Wireless Communications*, vol. 4, pp. 1759 – 1772, July 2005.

[38] Nabar, R., Erceg, V., Bolcskei, H., and Paulraj, A., "Performance of multiantenna signalling strategies using dual-polarized antennas: Measurement results and analysis," *Wireless Personal Communications*, vol. 23, pp. 31–44, Nov. 2002.

[39] Paulraj, A., Nabar, R., and Gore, D., *Introduction to Space-Time Wireless Communications*. Cambridge Univ. Press, 2nd ed., 2003.

[40] Perez, J., Ibaenez, J., Vielva, L., and Santamaria, I., "Approximate closed-form expression for the ergodic capacity of polarization diversity MIMO systems," *IEE Electronic Letters*, vol. 40, Sept 2004.

[41] Sanayei, S. and Nosratinia, A., "Capacity maximizing algorithms for joint transmit-receive antenna selection," *Asilomar Conference on Signals, Systems and Computers*, vol. 2, pp. 1773–1776, Nov 2004.

[42] Shiu, D.-S., Foschini, G., Gans, M., and Kahn, J., "Fading correlation and its effect on the capacity of multielement antenna systems," *IEEE Transactions on Communications*, vol. 48, pp. 502–513, March 2000.

[43] Stuber, G., *Principles of Mobile Communication*. Kluwer Academic Publishers, 2 ed., 2001.

[44] Sudarshan, P., Mehta, N., Molisch, A., and Zhang;, J., "Antenna selection with RF pre-processing: robustness to RF and selection non-idealities," *Radio and Wireless Conference, 2004 IEEE*, pp. 391–394, Sept 2004.

[45] Tan, C., Nix, A., and Beach, M., "Dynamic spatial-temporal propagation measurement and super-resolution channel characterisation at 5.2 GHz in a corridor environment," in *Proc. IEEE Vehicular Technology Conference (VTC)*, vol. 2, pp. 797–801, Sept. 2002.

[46] Tang, J., Zhang, X., and Du, Q., "Alamouti scheme with joint antenna selection and power allocation over Rayleigh fading channels in wireless networks," *IEEE Global Telecommunications Conference*, pp. 3319–3323, Nov 2005.

[47] Tarokh, V., Seshadri, N., and Calderbank, A., "Space-time codes for high data rate wireless communication: performance criterion and code construction," *IEEE Transactions on Information Theory*, vol. 44, pp. 744 – 765, March 1998.

[48] Vaughan, R. G., "Polarization diversity for mobile communications," *IEEE Transactions of Vehicular Technology*, vol. 39, August 1990.

[49] Wallace, J., Jensen, M., and A.L, S., "Experimental characterization of the MIMO wireless channel: data acquisition and analysis," *IEEE Transactions on Wireless Communications*, vol. 2, pp. 335–343, March 2003.

[50] Wheeden, R. and Zygmung, A., *Measure and Integral*. Marcel Dekker Inc, 1st ed., 1977.

[51] Zhao, X., Geng, S., Vuokko, L., Kivinen, J., and Vainikainen, P., "Polarization behaviors at 2, 5 and 60 GHz for indoor mobile communications," *Wireless Personal Communications*, vol. 27, pp. 99–115, Nov. 2003.

VITA

Vikram Reddy Anreddy was born in the southern Indian city of Hyderabad, on November 17, 1982. He received his Bachelor of Technology degree in Electronics and Communication Engineering, from the Indian Institute of Technology, Guwahati, India, in May 2004. He then attended the Master of Science program in the School of Electrical and Computer Engineering at the Georgia Institute of Technology, Atlanta, USA, from August 2004 to April 2006. At the same time, he worked as a graduate research assistant in the Smart Antennas Research Laboratory (SARL) at the Georgia Institute of Technology, under the guidance of Professor Mary Ann Ingram. Here his research focused on compact MIMO systems and LEO satellite communications. During the summers of 2003 and 2004, he worked as an intern, at the FTW Telecommunications Research Center Vienna, Austria.